

# Time resolution of silicon pixel sensors

W. Riegler, G. Aglieri Rinella

*CERN EP, CH-1211 Geneve 23*

---

## Abstract

We derive expressions for the time resolution of silicon detectors, using the Landau theory and a PAI model for describing the charge deposit of high energy particles. First we use the centroid time of the induced signal and derive analytic expressions for the three components contributing to the time resolution, namely charge deposit fluctuations, noise and fluctuations of the signal shape due to weighting field variations. Then we derive expressions for the time resolution using leading edge discrimination of the signal for various electronics shaping times. Time resolution of silicon detectors with internal gain is discussed as well.

*Keywords:* Charge induction; Charge transport and multiplication in solid media; Detector modelling and simulations I (interaction of radiation with matter, interaction of photons with matter, interaction of hadrons with matter, etc); Detector modelling and simulations II (electric fields, charge transport, multiplication and induction, pulse formation, electron emission, etc); Si microstrip and pad detectors; Solid state detectors; Timing detectors;

---

## Contents

<b>1</b>	<b>Introduction</b>	<b>3</b>
<b>2</b>	<b>Energy deposit</b>	<b>3</b>
<b>3</b>	<b>Centroid time of a signal</b>	<b>6</b>
<b>4</b>	<b>Silicon sensors without internal gain</b>	<b>7</b>
4.1	Centroid time resolution of a silicon detector signal . . . . .	7
4.2	Multiple particles passing a silicon sensor . . . . .	9
4.3	Noise contribution to the centroid time resolution . . . . .	11
4.4	Weighting field effect on the centroid time for uniform charge deposit . . . . .	16
4.5	Centroid time resolution for combined charge fluctuations and weighting field fluctuations	20
4.6	Leading edge discrimination . . . . .	23
<b>5</b>	<b>Silicon sensors with internal gain</b>	<b>26</b>
5.1	Centroid time resolution for silicon sensors with internal gain . . . . .	26
5.2	Weighting field effect on the centroid time for silicon sensors with gain . . . . .	28
5.3	Impact of gain fluctuations . . . . .	29
5.4	Leading edge discrimination for silicon sensors with gain . . . . .	30
<b>6</b>	<b>Comparison with measurements</b>	<b>31</b>
<b>7</b>	<b>Conclusions</b>	<b>32</b>
	<b>Appendix A</b>	<b>34</b>
	<b>Appendix B</b>	<b>35</b>
	<b>Appendix C</b>	<b>37</b>
	<b>Appendix D</b>	<b>37</b>
	<b>Appendix E</b>	<b>38</b>

## 1. Introduction

Silicon pixel sensors providing precise timing are currently being developed in view of future "4D" tracking applications. The NA62 Gigatracker, using sensors of  $200\text{ }\mu\text{m}$  thickness and  $300\text{ }\mu\text{m}\times 300\text{ }\mu\text{m}$  pixel size has achieved time resolutions of  $\leq 150\text{ ps}$  at rates of up to  $1.5\text{ MHz/cm}^2$  [1][2][3][4]. A time resolution of  $100\text{ ps}$  has been reported with a sensor of  $100\text{ }\mu\text{m}$  thickness and  $800\text{ }\mu\text{m}\times 800\text{ }\mu\text{m}$  pixel size [5]. For multiple particles passing silicon sensors of thickness between  $133$  and  $285\text{ }\mu\text{m}$ , a time resolution of better than  $20\text{ ps}$  has been reported [6]. With the introduction of internal amplification inside silicon detectors of  $50\text{ }\mu\text{m}$  thickness, the so called Low Gain Avalanche Diode (LGAD) [7][8][9][10][11], time resolutions of  $25\text{ ps}$  have been achieved for single MIPs [12].

The Weightfield2 program [13] allows the detailed simulation of the induced signals in silicon sensors with strip geometry. A long term goal of these developments are pixel sensors of  $10\text{ }\mu\text{m}$  position resolution and  $10\text{ ps}$  time resolution [14][15]. Developments of silicon sensors for increased timing performance based on 3D sensors are also described in literature [16]. Studies of front-end electronics for silicon detectors with emphasis on timing aspects can be found in [17] and [18]. Charged particle imaging is widely employed in many areas of science beyond high energy physics, for example as part of material analysis techniques. Therefore there is a broad interest in the developments of spatially resolved and time accurate particle detectors [19][20].

In this report we derive analytic expressions for the time resolution of silicon sensors using the Landau theory and a version of the PAI model to describe the charge deposit of high energy particles in the sensor. We first investigate the time resolution for the case where we take the 'centroid time' of the signal as a measure of time. It refers to the case where the amplifier peaking time is larger than the drift time of the electrons and holes in the silicon sensor and allows us to discuss the achievable time resolution using moderate electronics bandwidth together with optimum filter methods to extract the time information from the known signal shape. We then derive formulas quantifying the effect of signal fluctuations due to the finite pixel size and related variations of the weighting field. We also derive expressions for the time resolution using leading edge discrimination of the signals with different electronics shaping times. In the last part of the report we discuss the time resolution of silicon sensors with internal amplification which will be applied in the ATLAS and CMS experiment upgrades for pileup rejection [8].

## 2. Energy deposit

A high energy particle passing a silicon sensor will experience a number of primary interactions with the material, with  $\lambda$  being the average distance between these primary interactions. For relativistic particles we have  $\lambda \approx 0.212\text{ }\mu\text{m}$  in silicon [21]. The electrons created in these primary interactions will typically lose their energy over very small distances and create a localised cluster of electron-hole pairs. We call the probability  $p_{clu}(n)$  for creating  $n$  e-h pairs in a primary interaction the 'cluster-size distribution'. Throughout this report we treat  $n$  as a continuous variable. We now divide the silicon sensor of thickness  $d$  into  $N$  slices of thickness  $\Delta z = d/N$  as shown in Fig. 1a. In case  $\Delta z \ll \lambda$ , the probability for having zero interactions in  $\Delta z$  is  $1 - \Delta z/\lambda$ , the probability to have one interaction in  $\Delta z$  is  $\Delta z/\lambda$  and the probability to have more than one interaction is negligible, so the probability density for finding  $n$  electrons in  $\Delta z$  is

$$p(n, \Delta z)dn = \left(1 - \frac{\Delta z}{\lambda}\right) \delta(n)dn + \frac{\Delta z}{\lambda} p_{clu}(n)dn \quad (1)$$

The probability  $p(n, d)$  to have  $n$  electrons in the entire sensor of thickness  $d$  is then given by the  $N$  times self convolution of this expression. Since convolution becomes multiplication if we perform the Laplace

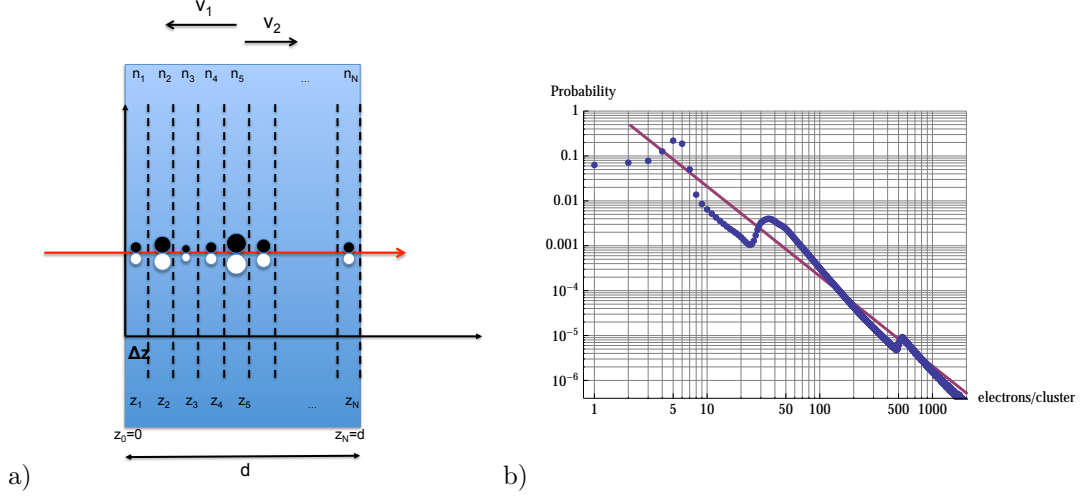


Figure 1: a) The silicon sensor is divided into slices of thickness  $\Delta z$ . The electrons and holes produced in one slice are assumed to move to the boundary of the sensor at constant velocity, which is correct in the limit of negligible depletion voltage. b) Probability to find  $n$  electrons per primary interaction. The straight line refers to the  $1/n^2$  distribution that is the basis for the Landau distribution, the points corresponds to a PAI model [21][22].

transform,  $N$  times self convoluting the above expression results in raising it's Laplace transform to the power  $N$ . So using the Laplace transform  $P_{clu}(s) = \mathcal{L}[p_{clu}(n)]$  we have

$$P(s, d) = \mathcal{L}[p(n, d)] = \mathcal{L}[p(n, \Delta z)]^N = \left(1 + \frac{d}{\lambda N} (P_{clu}(s) - 1)\right)^N \quad (2)$$

By taking the limit of  $N \rightarrow \infty$  we have

$$p(n, d) = \mathcal{L}^{-1} \left[ e^{d/\lambda (P_{clu}(s) - 1)} \right] \quad (3)$$

This expression is completely general and correct for any cluster size distribution. Assuming as an (unphysical) example that each cluster contains exactly  $n_0$  electrons we have

$$p_{clu}(n) = \delta(n - n_0) \quad P_{clu}(s) = e^{-s n_0} \quad P(n, s) = e^{d/\lambda (e^{-n_0 s} - 1)} \quad (4)$$

The inverse Laplace transform of the last expression is

$$p(n, d) = \sum_{k=0}^{\infty} \frac{\left(\frac{d}{\lambda}\right)^k}{k!} e^{-\frac{d}{\lambda}} \delta(n - k n_0) \quad \mu = n_0 d / \lambda \quad \frac{\Delta}{\mu} = \frac{1}{\sqrt{d/\lambda}} \quad (5)$$

where  $\mu$  is the average number of e-h pairs and  $\Delta$  is the standard deviation. This is the expected Poisson distribution showing the  $1/\sqrt{N}$  dependence for the relative fluctuations with  $N = d/\lambda$  being the average number of clusters.

The correct cluster size distribution  $p_{clu}(n)$  is typically calculated using some form of the PAI model [22] and an example is shown in Fig. 1b [21]. For this report we also use the Landau theory as a minimal model that respects basic physics and that allows approximate analytic expressions. Landau's approach assumes a  $1/E^2$  distribution of the energy transfer for a collision in accordance with Rutherford scattering on free electrons and a lower cutoff energy  $\epsilon$  chosen such that the average energy loss reproduces the Bethe-Bloch

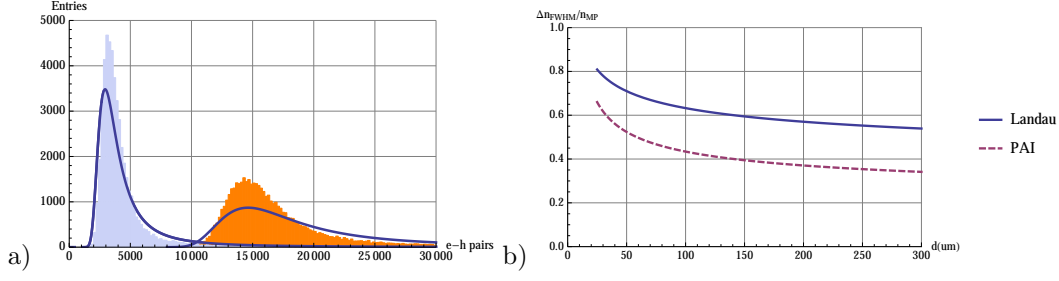


Figure 2: a) Distribution of the number of e-h pairs in 50  $\mu\text{m}$  (blue) and 200  $\mu\text{m}$  (orange) of silicon. The histograms show the PAI model, the solid lines show the Landau theory. b) Ratio of full width half maximum and most probable values for the Landau and PAI model for different values of silicon thickness. The Landau theory overestimates the fluctuations by 25-35%.

theory. The resulting cluster size distribution for a MIP in silicon therefore becomes a  $1/n^2$  distribution with a cutoff at  $n = n_0 \approx 2.2$  electrons, which can be written as

$$p_{clu}(n) \approx \frac{n_0}{n^2} \Theta(n - n_0) \quad P_{clu}(s) \approx 1 + n_0 s (C_\gamma - 1 + \ln n_0 + \ln s) \quad (6)$$

with  $\Theta(x)$  being the Heaviside step function. Evaluating Eq. 3 results in

$$p(n, d) dn = \frac{\lambda}{n_0 d} L\left(\frac{\lambda}{n_0 d} n + C_\gamma - 1 - \ln \frac{d}{\lambda}\right) dn \quad (7)$$

where  $C_\gamma = 0.5772\dots$  is the Euler-Mascheroni constant and  $L(x)$  is the Landau distribution discussed in Appendix A. The most probable number of e-h pairs  $n_{MP}$  and the full width of half maximum  $n_{FWHM}$  of  $p(n, d)$  are

$$n_{MP} \approx \frac{n_0 d}{\lambda} \left(0.2 + \ln \frac{d}{\lambda}\right) \quad \frac{\Delta n_{FWHM}}{n_{MP}} \approx \frac{4.02}{0.2 + \ln d/\lambda} \quad (8)$$

It should be noted that the most probable number of electrons  $n_{MP}$  is proportional to the cutoff  $n_0$  while the ratio of  $n_{FWHM}$  and  $n_{MP}$  is independent of  $n_0$  and depends only on  $d/\lambda$ .

For a value of  $\lambda = 0.212 \mu\text{m}$  we find an average of  $N = d/\lambda = 236, 472, 943, 1415$  primary interactions (clusters) for a 50, 100, 200, 300  $\mu\text{m}$  silicon sensor. Using the cluster size distribution from Eq. 6, the probability that at least one of the  $N$  clusters contains more than  $n_1$  electrons is given by

$$p_{>n_1} = 1 - \left(1 - \frac{n_0}{n_1}\right)^N \quad (9)$$

so there is still a 1% chance to have a cluster with more than  $n_1 = 73500, 103000, 206000, 309000$  electrons for a single MIP passing a 50, 100, 200, 300  $\mu\text{m}$  silicon sensor! When performing Monte Carlo simulations, the cut-off of the cluster size distribution has therefore to be placed beyond these numbers. The primary electrons producing these large clusters are called delta-electrons and do not deposit their charge at point-like clusters but short tracks, which has to be considered when discussing pixels of small size.

Fig. 2a shows the distribution of e-h pairs in a 50  $\mu\text{m}$  and a 200  $\mu\text{m}$  sensor for the PAI model together with the curves from the Landau theory. As seen in Fig. 2b the Landau theory overestimates the fluctuations by 25-35%. The PAI model predicts a most probable number of 3160, 6710, 14200, 21900 e-h pairs in 50, 100, 200, 300  $\mu\text{m}$  of silicon, which is within 10% of the values from the Landau theory when assuming a cutoff of  $n_0 = 2.2$ . We will use both models for evaluation of the time resolution in the following.

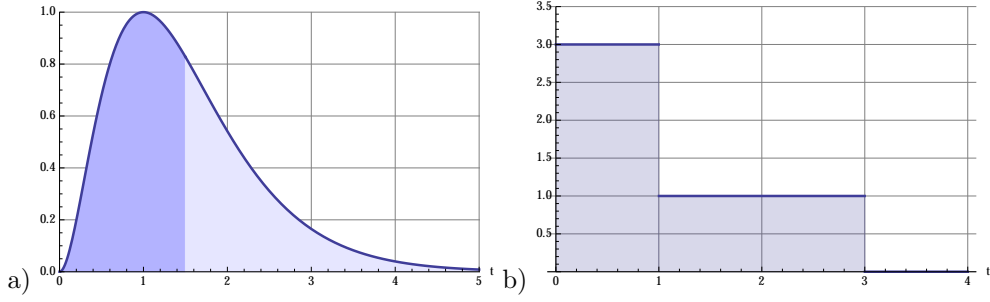


Figure 3: a) The centroid time  $\tau$  of a signal is defined as the time where signal integral (area) for  $t < \tau$  and  $t > \tau$  is balanced. b) Example of the signal from a single e-h pair in a silicon sensor with negligible depletion voltage.

### 3. Centroid time of a signal

First we assume the measured time to be defined by the centroid time of the induced detector current signal  $i(t)$  (Fig. 3a. Assuming the Laplace Transform of the signal  $I(s) = \mathcal{L}[i(t)]$ , the centroid time  $\tau_{cur}$  of the signal is defined by

$$\tau_{cur} = \frac{\int_0^\infty t i(t) dt}{\int_0^\infty i(t) dt} = \frac{\int_0^\infty t i(t) dt}{q} = -\frac{I'(0)}{I(0)} \quad (10)$$

where  $q = \int_0^\infty i(t) dt$  is the total signal charge. If we consider the signal  $i(t)$  to be processed by an amplifier having a delta response  $f(t)$  with Laplace Transform  $F(s)$ , the amplifier output signal  $v(t)$  is given by

$$v(t) = \int_0^t f(t-t') i(t') dt' \quad V(s) = F(s) I(s) \quad (11)$$

The centroid time of the output signal is then

$$\tau_v = -\lim_{s \rightarrow 0} \frac{V'(s)}{V(s)} = -\frac{F'(0)I(0) + F(0)I'(0)}{F(0)I(0)} = -\frac{F'(0)}{F(0)} - \frac{I'(0)}{I(0)} = \tau_{amp} + \tau_{cur} \quad (12)$$

This represents the sum of the centroid time of the delta response and the one from the current signal, and since the shape of the delta response does not vary in time, the centroid time variation of the amplifier output signal is equal to the centroid time variation of the original input signal and has no dependence on the amplifier characteristics.

To determine  $\tau$  by recording the signal shape and performing the integral of Eq. 10 is not very practical, it is easier to simply process the signal with an amplifier that is 'slow' compared to the signal duration, as shown in the following. In case the duration  $T$  of the signal  $i(t)$  is short compared to the 'peaking time'  $t_p$  of the amplifier ( $i(t) = 0$  for  $t > T \ll t_p$ ) we can approximate Eq. 11 for  $t > T$  according to

$$\begin{aligned} v(t) &= \int_0^T f(t-t') i(t') dt' \approx \int_0^T [f(t) - f'(t)t'] i(t') dt' \\ &= q \left[ f(t) - f'(t) \frac{\int_0^T t' i(t') dt'}{q} \right] = q [f(t) - f'(t) \tau_{cur}] \\ &\approx q f(t - \tau_{cur}) \end{aligned} \quad (13)$$

The amplifier output is simply equal to the amplifier delta response shifted by the centroid time of the current signal and scaled by the total charge of the signal. Since the shape of the amplifier output signal is always equal to the amplifier delta response, we can determine the signal centroid time either

by the threshold crossing time at a given fraction of the signal or by sampling the signal and fitting the known signal shape to the samples. For later use we remark that for the sum of two current signals  $i(t) = i_1(t) + i_2(t)$  with centroid times  $\tau_1$  and  $\tau_2$  we have

$$\tau = \frac{\int t i(t) dt}{\int i(t) dt} = \frac{\tau_1 \int i_1(t) dt + \tau_2 \int i_2(t) dt}{\int i_1(t) dt + \int i_2(t) dt} = \frac{\tau_1 q_1 + \tau_2 q_2}{q_1 + q_2} \quad (14)$$

The centroid time for the sum of  $N$  signals  $i(t) = \sum_{k=1}^N i_k(t)$  is therefore given by

$$\tau = \frac{1}{\sum_{k=1}^N q_k} \sum_{k=1}^N q_k \tau_k \quad (15)$$

where  $q_k$  and  $\tau_k$  are the charges and centroid times of the individual signals  $i_k(t)$ .

#### 4. Silicon sensors without internal gain

##### 4.1. Centroid time resolution of a silicon detector signal

We assume a silicon sensor operated at large over-depletion i.e. at a voltage that is large compared to the depletion voltage and the electric field can therefore be assumed to be constant throughout the sensor. Consequently the velocities of electrons and holes are constant and the signal from a single electron or single hole has a rectangular shape. We assume a parallel plate geometry with one plate at  $z = 0$  and one at  $z = d$ , where a pair of charges  $+q, -q$  is produced at position  $z$  and  $-q$  moves with velocity  $v_1$  to the electrode at  $z = 0$  while  $q$  moves with velocity  $v_2$  to the electrode at  $z = d$ . The weighting field of the electrode at  $z = 0$  is  $E_w = 1/d$  and the induced current is therefore

$$i(t) = -\frac{qv_1}{d} \Theta(z/v_1 - t) - \frac{qv_2}{d} \Theta((d-z)/v_2 - t) \quad (16)$$

with  $\Theta(t)$  being the Heaviside step function. An example is shown in Fig. 3b. We have  $\int i(t) dt = -q$  and according to Eq. 10 the centroid time of this signal is then

$$\tau = \frac{1}{2d} \left[ \frac{z^2}{v_1} + \frac{(d-z)^2}{v_2} \right] \quad (17)$$

If  $n_1, n_2, \dots, n_N$  charges are produced at positions  $z_1, z_2, \dots, z_N$  and are moving to the electrodes with  $v_1$  and  $v_2$ , the resulting centroid time of the signal is

$$\tau(n_1, n_2, \dots, n_N) = \frac{1}{2d (\sum_{k=1}^N n_k)} \sum_{k=1}^N n_k \left[ \frac{z_k^2}{v_1} + \frac{(d-z_k)^2}{v_2} \right] \quad (18)$$

We now divide the sensor of thickness  $d$  into  $N$  slices of  $\Delta z = d/N$  as shown in Figure 1. The probability to have  $n_k$  e/h pairs in slice  $k$  is given by the Landau distribution  $p(n_k, \Delta z)$  and if we assume that all these charges are moving from position  $z_k$  to the electrodes, we have  $z_k = k \Delta z$  and we can proceed to calculate the variance  $\Delta_\tau^2$  of the centroid time of the signal, i.e. the time resolution, according to

$$\Delta_\tau^2 = \overline{\tau^2} - \bar{\tau}^2 \quad (19)$$

with  $\bar{\tau}$  and  $\overline{\tau^2}$  being the average and the second moment of  $\tau$ . The evaluation is given in Appendix B and we find

$$\Delta_\tau = w(d) \sqrt{\frac{4}{180} \frac{d^2}{v_1^2} - \frac{7}{180} \frac{d^2}{v_1 v_2} + \frac{4}{180} \frac{d^2}{v_2^2}} \quad (20)$$

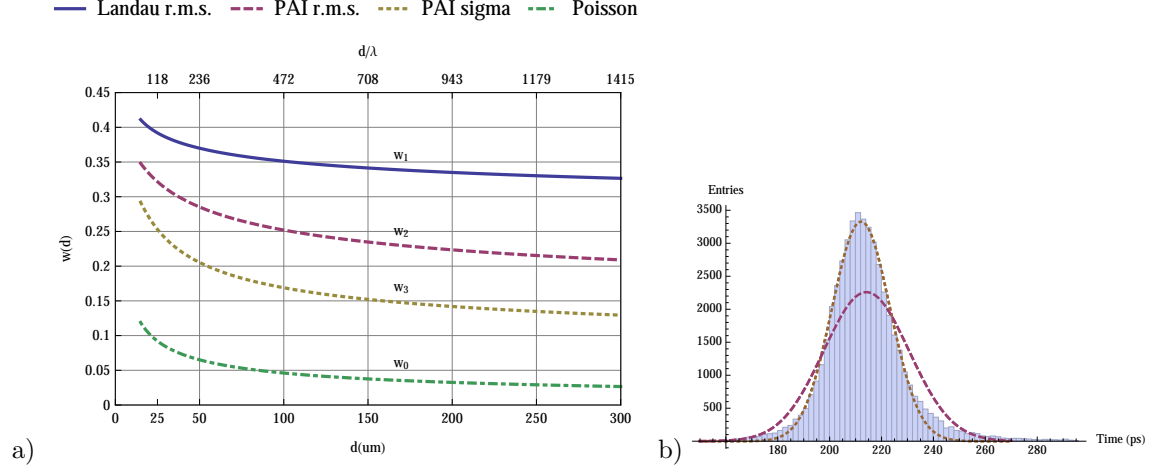


Figure 4: a) The function  $c(d)$  for different values of silicon thickness.  $w_1$  represents the Landau theory,  $w_2$  represents the PAI model and  $w_3$  applies for the PAI model if we use a Gaussian fit instead of the r.m.s. as a measure of the time resolution. b) Centroid time distribution for  $d = 50 \mu\text{m}$  and  $V = 220 \text{ V}$  for the PAI model. The dashed curve represents a Gaussian with a  $\sigma = \Delta_\tau$  ( $w_2$ ) and the dotted curve is a Gaussian fit to the histogram ( $w_3$ ).

with

$$w(d)^2 = \frac{d}{\lambda} \int_0^\infty \left[ \int_0^\infty \frac{n_1^2 p_{clu}(n_1)}{(n_1 + n)^2} dn_1 \right] p(n, d) dn \quad (21)$$

We first evaluate the expression for the (unphysical) case where we assume each cluster to have exactly  $n_e$  electrons i.e.  $p_{clu}(n) = \delta(n - n_e)$ . The expression inside the square brackets then evaluates to  $n_e^2 / (n_e + n)^2$ . The probability  $p(n, d)$  to find  $n$  electrons in  $d$  is the Poisson distribution from Eq. 5 with it's peak at  $n = N n_e$ . Since the above expression does not vary significantly within the width of the Poisson distribution, the integral can be approximated by evaluating the expression at  $n = N n_e$ , and we have

$$w(d) \approx \sqrt{N \frac{n_e^2}{(n_e + N n_e)^2}} \approx \frac{1}{\sqrt{N}} = \frac{1}{\sqrt{d/\lambda}} \quad (22)$$

This is a very intuitive result related to the typical behaviour of the relative fluctuation of the Poisson distribution. The evaluation of  $w(d)$  for the Landau theory is given in Appendix C with the result that for large values of  $d/\lambda$  we have

$$w(d) \approx \frac{1}{\sqrt{\ln d/\lambda}} \quad (23)$$

The value of  $w(d)$  is given in Fig. 4a for the Poisson case ( $w_0$ ), the Landau theory ( $w_1$ ), the PAI model ( $w_2$ ) and for the case where we do not use the r.m.s. value but a Gaussian fit to the measured times as a measure of the time resolution ( $w_3$ ). As shown in Fig. 4b the time distribution has very large tails, so the r.m.s. and a Gaussian fit differ significantly. The three curves  $w_1, w_2, w_3$  are parametrized in the range of  $15 \mu\text{m} < d < 300 \mu\text{m}$  as

$$w(d) \approx \frac{1}{\sqrt{a + b \ln d/\lambda + c (\ln d/\lambda)^2}} \quad (24)$$

with  $a_1 = 1, b_1 = 1.155, c_1 = 0, a_2 = 13.7, b_2 = -4.9, c_2 = 0.85, a_3 = 47.7, b_3 = -22.8, c_3 = 3.37$ . The function  $w(d)$  shows only a weak dependence on  $d$ , like the relative width  $n_{FWHM}/n_{MP}$  from Eq. 8.



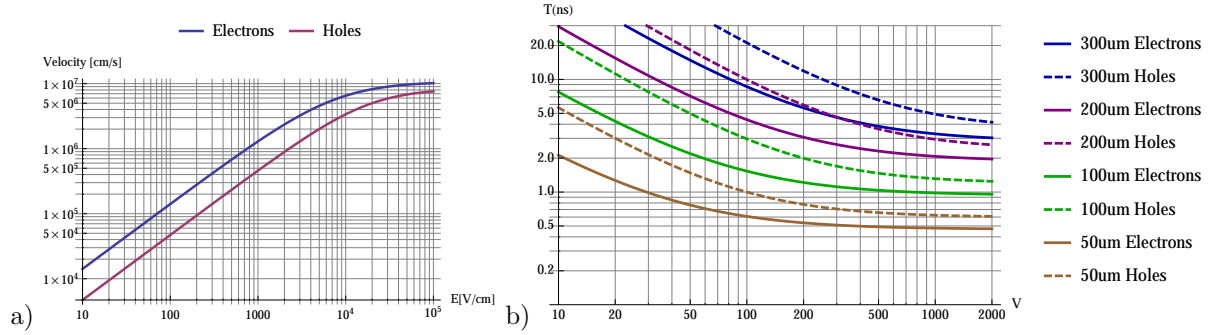


Figure 5: a) Velocity of electrons and holes as a function of electric field. b) Time for electrons and holes to transit the full thickness of the sensor assuming negligible depletion voltage.

When going from a 50  $\mu\text{m}$  to a 300  $\mu\text{m}$  sensor this statistical effect improves only by 20-30 %.

Neglecting this weak dependence on  $d$ , the time resolution at constant electric field i.e. at constant drift velocity  $v_1$  and  $v_2$  scales with  $d$ , which represents the trivial fact that the duration of the signal and therefore also  $\Delta\tau$  scales with  $d$ . For a given voltage  $V$ , the electric fields in the thinner sensors, and therefore the velocities of electrons and holes are of course larger, so the time resolution improves significantly beyond the  $1/d$  scaling for thin sensors.

If we associate  $v_1$  and  $v_2$  with the electron and hole velocity,  $T_1 = d/v_1$  and  $T_2 = d/v_2$  are the total drift times of electrons and holes, and  $T_{12} = d/\sqrt{v_1 v_2}$  is the total drift time assuming the geometric mean of the electron and hole velocity, and the time resolution reads as

$$\Delta\tau = w(d) \sqrt{4/180} \sqrt{T_1^2 - 1.75 T_{12}^2 + T_2^2} \quad (25)$$

To get realistic estimates we use an approximation for the velocity of the electrons and holes from [26]

$$v_e(E) = \frac{\mu_e E}{\left[1 + \left(\frac{\mu_e E}{v_{sat}^e}\right)^{\beta_e}\right]^{1/\beta_e}} \quad v_h(E) = \frac{\mu_h E}{\left[1 + \left(\frac{\mu_h E}{v_{sat}^h}\right)^{\beta_h}\right]^{1/\beta_h}} \quad (26)$$

where we chose  $\mu_e = 1417 \text{ cm}^2/\text{Vs}$ ,  $\mu_h = 471 \text{ cm}^2/\text{Vs}$ ,  $\beta_e = 1.109$ ,  $\beta_h = 1.213$  and  $v_{sat}^e = 1.07 \times 10^7 \text{ cm/s}$  and  $v_{sat}^h = 0.837 \times 10^7 \text{ cm/s}$  at 300 K in accordance with the default models in Sentaurus Device [23]. The resulting drift velocity together with the time that the electrons and holes need to traverse the sensor (assuming  $V_{dep} = 0$ ) are given in Fig. 5. For a 50  $\mu\text{m}$  sensor at 200 V the electrons take 0.6 ns and the holes take 0.8 ns to traverse the sensor, so the total signal duration is  $< 0.8 \text{ ns}$ .

The values for the time resolution according to Eq. 20 for the Landau theory, the PAI model and a Gaussian fit to the PAI model are given in Fig. 6 for 50, 100, 200 and 300  $\mu\text{m}$  sensors. A 200  $\mu\text{m}$  sensor can achieve a time resolution of  $< 50 \text{ ps}$  for  $V > 350 \text{ V}$  and a 50  $\mu\text{m}$  sensor can achieve  $< 15 \text{ ps}$  for  $V > 200 \text{ V}$ .

#### 4.2. Multiple particles passing a silicon sensor

In [6] the time resolution for multiple particles crossing a sensor is discussed. The case of  $n$  particles passing the silicon sensor is equivalent to the situation of one particle passing the sensor with a mean free path between collisions reduced to  $\lambda_n = \lambda/n$ . According to the Landau theory we have  $w(d) \approx 1/\sqrt{\ln d/\lambda}$  for a single particle, so for  $n$  particles the fluctuations reduce according to

$$\frac{\Delta\tau(n \text{ particles})}{\Delta\tau(1 \text{ particle})} = \frac{1}{\sqrt{1 + \frac{\ln n}{\ln d/\lambda}}} \quad (27)$$

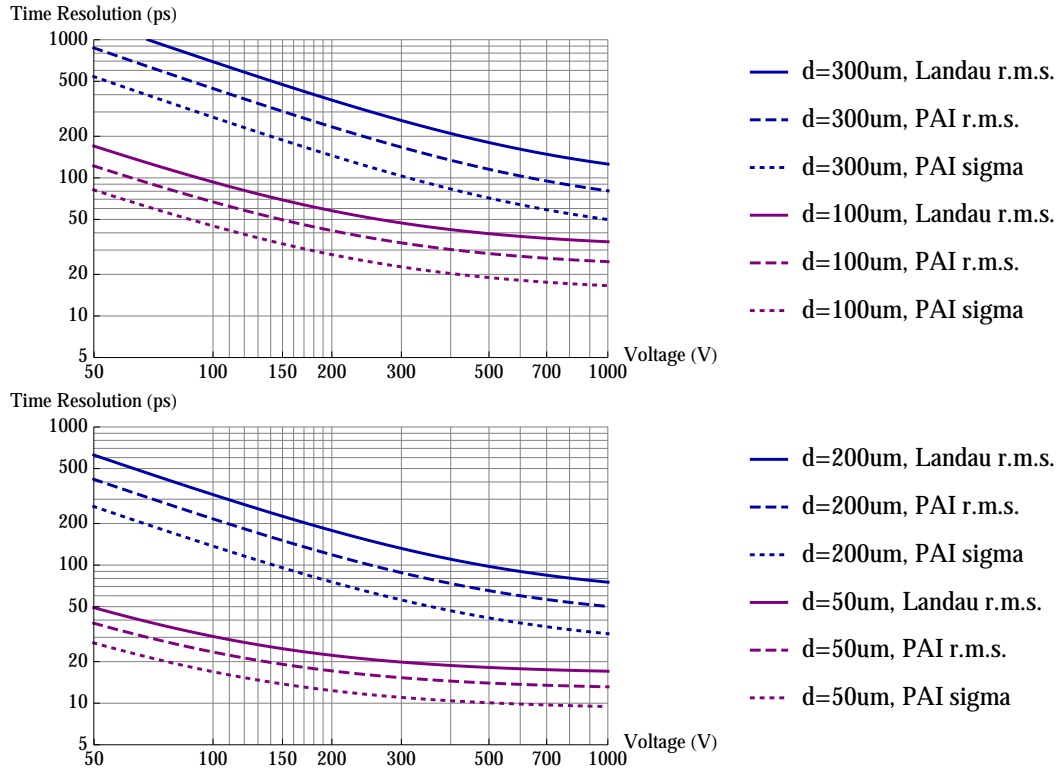


Figure 6: Time resolution from Eq. 20 for different values of silicon sensor thickness as a function of applied voltage  $V$  for the Landau model, the PAI model and a Gaussian fit to the PAI model results.

This function has an extremely weak dependence on  $n$  so the improvement of the centroid time resolution when going from 1 to 100 particles for a 50/100/200/300  $\mu\text{m}$  sensor is only 26/24/23/22 %. The centroid time resolution does therefore not significantly change for multiple particles. The signal to noise ratio does however improve almost linearly with the number of particles passing the sensor, so when using leading edge discrimination with a threshold set close to the noise level as discussed in Section 4.6, there is in principle no lower bound on the time resolution.

#### 4.3. Noise contribution to the centroid time resolution

As shown in Eq. 13 the centroid time of a signal can be measured by using an amplifier with a peaking time  $t_p$  that is larger than the total signal time  $T$ . For a 50  $\mu\text{m}$  sensor at 250 V this signal time is  $T \approx 0.8$  ns, so an amplifier with peaking time  $t_p > 1.5$  ns can realise such a measurement. The problem to solve is therefore to measure the time of a pulse of known shape (the delta response) that has noise of a known frequency spectrum superimposed. This can be accomplished by various techniques of constant fraction discrimination or continuous sampling with optimum filtering methods, both of which will be discussed in this section. For the remainder of the report we assume an unipolar amplifier with a delta response of

$$f(t) = \left(\frac{t}{t_p}\right)^n e^{n(1-t/t_p)} \Theta(t) \quad (28)$$

where  $t_p$  is the peaking time and  $\Theta(t)$  is the Heaviside step function. The delta response for  $n = 2, 3, 4$  is shown in Fig. 7a. Such an amplifier can be realized by  $n$  integration stages with  $\tau = RC = t_p/n$  and for large values of  $n$  it approaches Gaussian shape (semi-gaussian shaping). In general we can use it to parametrize a measured delta response shape by adjusting  $n$  and  $t_p$  to fit a specific amplifier delta response. The normalized transfer function and related 3 dB bandwidth frequency  $f_{bw}$  of the above delta response are given by

$$|W(i2\pi f)| = \frac{1}{\sqrt{[1 + (2\pi f)^2 t_p^2 / n^2]^{n+1}}} \quad f_{bw} = \frac{1}{2\pi t_p} n \sqrt{2^{1/(n+1)} - 1} \quad (29)$$

For constant fraction discrimination we set the threshold to a value where  $f(t)$  has the maximum slope of  $f'(t_s)$  at time  $t_s$  which evaluates to

$$t_s = t_p (1 - 1/\sqrt{n}) \quad f'(t_s) = \frac{1}{t_p} e^{\sqrt{n}} n^{(3/2-n)} (n - \sqrt{n})^{n-1} \quad (30)$$

Assuming a pulse-height  $A$  and a noise of  $\sigma_{noise}$ , the timing error when applying the threshold at the maximum slope is then

$$\sigma_t = \frac{\sigma_{noise}}{A} \frac{1}{f'(t_s)} = \frac{\sigma_{noise}}{A} \frac{t_p}{e^{\sqrt{n}} n^{(3/2-n)} (n - \sqrt{n})^{n-1}} = \frac{\sigma_{noise}}{A} \frac{1}{2\pi f_{bw}} \frac{\sqrt{2^{1/(n+1)} - 1}}{e^{\sqrt{n}} n^{(1/2-n)} (n - \sqrt{n})^{n-1}} \quad (31)$$

as illustrated in Fig. 7b. This evaluates to

$$\begin{aligned} &= \frac{\sigma_{noise}}{A} t_p \times (0.59, 0.57, 0.54, 0.51) \quad \text{for} \quad n = 2, 3, 4, 5 \\ &= \frac{\sigma_{noise}}{A} \frac{1}{f_{bw}} \times (0.10, 0.12, 0.13, 0.14) \quad \text{for} \quad n = 2, 3, 4, 5 \end{aligned} \quad (32)$$

So for an amplifier with a peaking time of  $t_p = 1$  ns and  $n = 2$ , the time resolution is 60 ps for a signal to noise ratio of 10 and 20 ps for a signal to noise ratio of 30.

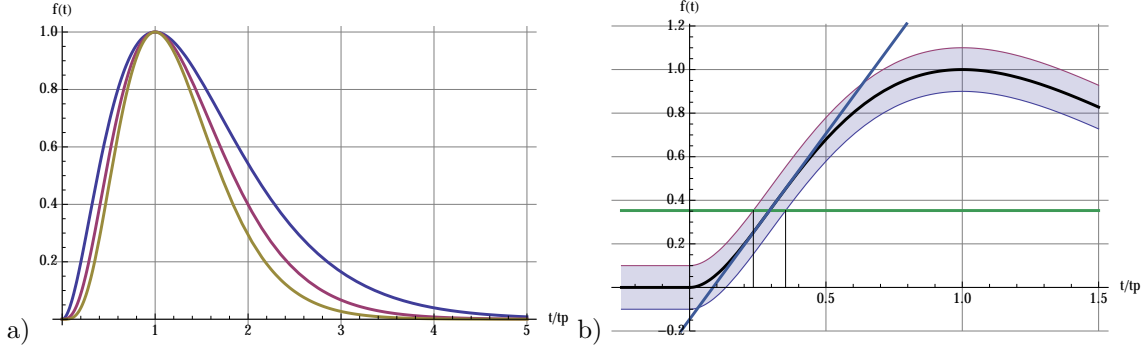


Figure 7: a) Amplifier response for  $n = 2, 3, 4$  from Eq. 28. b) Contribution to the time resolution from the noise.

The pulse-height of the silicon sensor signal is given by the total number  $n$  of deposited e-h pairs, so if we write the noise  $\sigma_{noise}$  in units of electrons, the average expression for  $\sigma_{noise}/A$  becomes

$$\frac{\sigma_{noise}}{A} = \int_0^\infty \frac{\sigma_{noise}}{n} p(n, d) dn \quad (33)$$

where  $p(n, d)$  is from Eq. 3. For the Landau theory we use Eq. C.2 to evaluate this expression to

$$\int_0^\infty \frac{\sigma_{noise}}{n} p(n, d) dn = \frac{\sigma_{noise}}{n_0 d} w_1(d)^2 \approx \frac{\sigma_{noise}}{n_0 d} \frac{1}{a_1 + b_1 \ln d/\lambda} \quad (34)$$

For the average time resolution we therefore find

$$\bar{\sigma}_t \approx \sigma_{noise} \frac{\lambda}{n_0 d} \frac{1}{1 + 1.155 \ln d/\lambda} t_p \times (0.59, 0.57, 0.54, 0.51) \quad \text{for } n = 2, 3, 4, 5 \quad (35)$$

$$\approx \sigma_{noise} \frac{\lambda}{n_0 d} \frac{1}{1 + 1.155 \ln d/\lambda} \frac{1}{f_{bw}} \times (0.10, 0.12, 0.13, 0.14) \quad \text{for } n = 2, 3, 4, 5 \quad (36)$$

For an average cluster distance of  $\lambda = 0.212 \mu m$ ,  $n_0 = 2.2$  and an amplifier with  $n = 2$ , this expression becomes

$$\sigma_t \approx \sigma_{noise}[\text{electrons}] \times 1.6 \times 10^{-4} t_p \quad d = 50 \mu m \quad (37)$$

$$\approx \sigma_{noise}[\text{electrons}] \times 3.3 \times 10^{-5} t_p \quad d = 200 \mu m \quad (38)$$

Assuming a  $50 \mu m$  sensor and a peaking time of 2 ns and an Equivalent Noise Charge (ENC) of 50 electrons, the noise contribution to the time resolution is 16.6 ps. Assuming a  $200 \mu m$  sensor and  $t_p = 10$  ns and ENC of 200 electrons, the contribution to the time resolution is 66 ps. The series noise of an amplifier for a given white series noise spectral density  $e_n^2$  and detector capacitance  $C$  is given by

$$\sigma_{noise}^2 = \frac{1}{2} e_n^2 C^2 \int_{-\infty}^\infty f'(t)^2 dt = \frac{1}{2} e_n^2 C^2 \frac{n^2 (2n-2)!}{t_p} \left( \frac{e}{2n} \right)^{2n} \quad (39)$$

For constant  $e_n^2$  the noise decreases with  $1/\sqrt{t_p}$  while the time resolution is proportional to  $t_p$ , so one favours short peaking times for minimizing the impact of noise, as long as other noise sources do not become dominant.

Since we know the shape of the delta response, continuous sampling of the signal and fitting of the

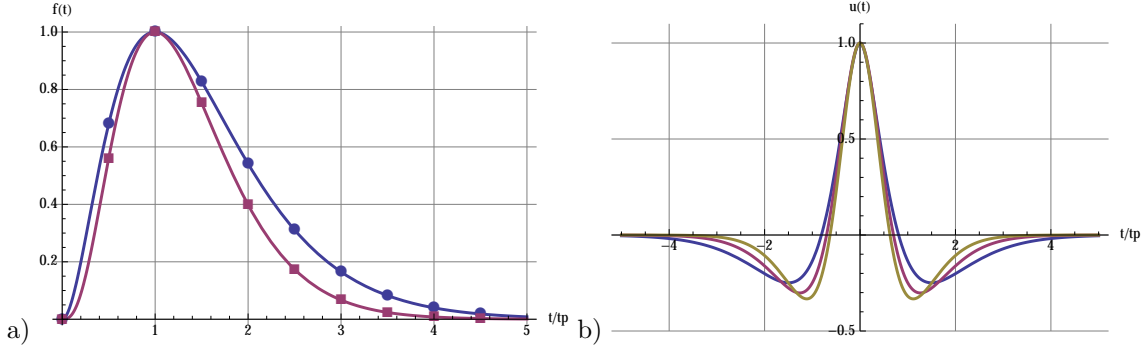


Figure 8: a) Sampling the signal at constant frequency. b) Autocorrelation function of  $f'(t)$  for  $n = 2, 3, 4$ . For times smaller than  $0.5 t_p$  the samples become highly correlated.

known shape to the sample points provides an effective way to determine the time as shown in Fig. 8a and investigated in the following. We have to fit the function  $A f(t - \tau)$  to the measured signal with the amplitude  $A$  and time  $\tau$  as free parameters. Linearizing this expression for small values of  $\tau$  we have

$$A f(t - \tau) \approx A f(t) - A f'(t) \tau = \alpha_1 f(t) - \alpha_2 f'(t) \quad \alpha_1 = A \quad \alpha_2 = A \tau \quad (40)$$

Finding the best estimate of  $\alpha_1, \alpha_2$  for a signal  $S_1, S_2, \dots, S_N$  sampled at times  $t_1, t_2, \dots, t_N$  leads to the familiar problem of linear regression. We proceed as outlined in [24] where the problem is stated as a  $\chi^2$  minimization according to

$$\chi^2 = \sum_{i=1}^N \sum_{j=1}^N [S_i - \alpha_1 f(t_i) + \alpha_2 f'(t_i)] V_{ij} [S_j - \alpha_1 f(t_j) + \alpha_2 f'(t_j)] \quad (41)$$

The matrix  $V_{ij}$  is the inverse of the autocorrelation matrix  $R_{ij} = R(t_i - t_j)$  with  $R(t)$  being the autocorrelation function of the series noise. The autocorrelation function of this series noise is

$$R(t) = \sigma_{noise}^2 \int_{-\infty}^{\infty} f'(t+u) f'(u) du = \sigma_{noise}^2 n! \left( \frac{2n|t|}{t_p} \right)^n \frac{2t_p K_{n-1/2}(n|t|/t_p) - t K_{n+1/2}(n|t|/t_p)}{(2n-2)! \sqrt{2n|t| t_p \pi}} \quad (42)$$

with  $K_\nu(x)$  being the modified Bessel function of the second kind. For  $n = 2, 3$  evaluates to

$$R(t) = \sigma_{noise}^2 U(t) = \sigma_{noise}^2 e^{-2|t|/t_p} \left[ 1 + 2 \frac{|t|}{t_p} - 4 \left( \frac{|t|}{t_p} \right)^2 \right] \quad n = 2 \quad (43)$$

$$= \sigma_{noise}^2 e^{-3|t|/t_p} \left[ 1 + 3 \frac{|t|}{t_p} - 9 \left( \frac{|t|}{t_p} \right)^3 \right] \quad n = 3 \quad (44)$$

The autocorrelation function is shown in Fig. 8b, and we see that for time intervals smaller than  $t_p/2$  the samples become highly correlated. In the following we use  $n_s$  samples within the peaking time  $t_p$ , so we have sampling time bins of  $\Delta t = t_p/n_s$ . We sample the signal in the range of  $0 < t < 5 t_p$ , giving  $t_i = i \Delta t$  with  $0 < i < 5 n_s$ . Defining

$$Q_1(n_s) = \sum_{ij} f(t_i) U_{ij}^{-1} f(t_j) \quad Q_2(n_s) = \sum_{ij} f'(t_i) U_{ij}^{-1} f'(t_j) \quad Q_3(n_s) = \sum_{ij} f'(t_i) U_{ij}^{-1} f(t_j) \quad (45)$$

where  $U_{ij}^{-1}$  is the inverse of the matrix  $U_{ij} = U(t_i - t_j)$ , the covariance matrix elements  $\varepsilon_{ij}$  for  $\alpha_1, \alpha_2$  are then

$$\varepsilon_{11} = \sigma_A^2 = \frac{\sigma_{noise}^2 Q_2}{Q_1 Q_2 - Q_3^2} \quad \varepsilon_{22} = A^2 \frac{\sigma_\tau^2}{t_p^2} = \frac{\sigma_{noise}^2 Q_1}{Q_1 Q_2 - Q_3^2} \quad \varepsilon_{12} = \frac{\sigma_{noise}^2 Q_3}{Q_1 Q_2 - Q_3^2} \quad (46)$$

So for the time resolution we finally have

$$\frac{\sigma_\tau}{t_p} = \frac{\sigma_{noise}}{A} \sqrt{\frac{Q_1(n_s)}{Q_1(n_s)Q_2(n_s) - Q_3(n_s)^2}} = \frac{\sigma_{noise}}{A} c(n_s) \quad (47)$$

Using as before the average signal to noise ratio for a sensor of thickness  $d$  we find

$$\overline{\sigma_t} = \sigma_{noise}[\text{electrons}] \frac{\lambda}{n_0 d} \frac{1}{1 + 1.155 \ln d/\lambda} t_p c(n_s) \quad (48)$$

This expression represents the optimum time resolution that can be achieved for a given sampling frequency. Fig. 9 shows the function  $c(n_s)$  assuming an amplifier with  $n = 2, 3$ . The horizontal lines correspond to the numbers of 0.59 and 0.57 from Eq. 35 when using constant fraction discrimination at the maximum slope. The families of curves represent a scan of the sampling phase with respect to the peak of the signal and the solid curve represents the average. The samples on the largest slope carry the highest weight on time information, while samples around the signal peak carry very little time information.

We see that sampling at an interval corresponding to half the peaking time ( $n_s = 2$ ) gives approximately the same result as the constant fraction discrimination at maximum slope. By increasing the sampling rate further the value cannot be improved much beyond a factor 2-3. This result is quite evident, since the noise is highly correlated on a timescale of  $< t_p/2$  as seen from Fig. 8b, so further increase of the sampling rate does not provide more information.

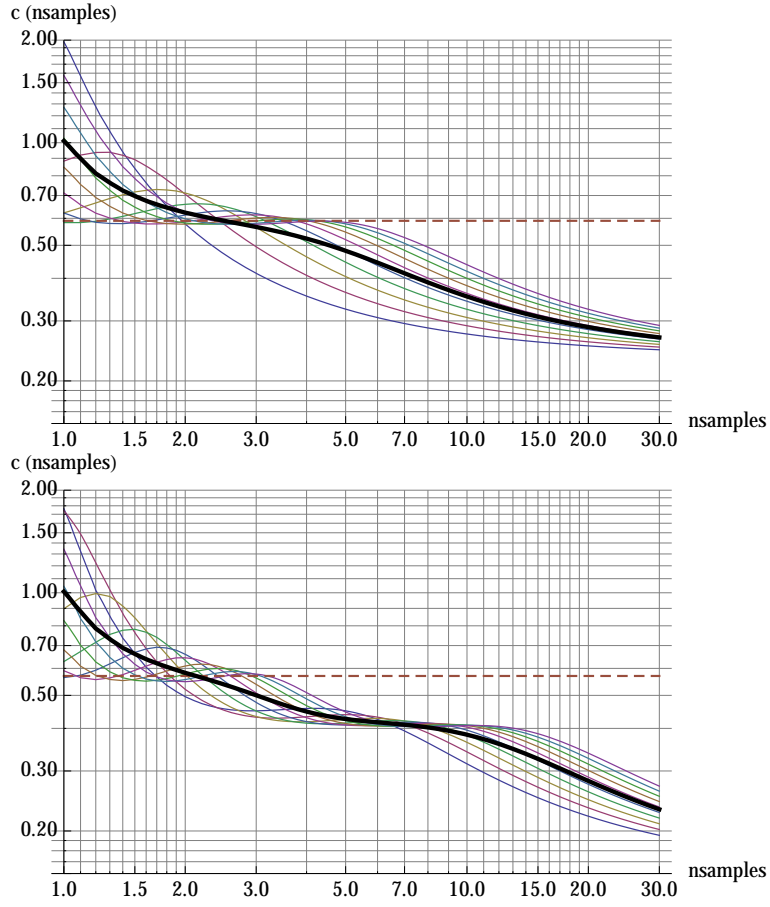


Figure 9: The function  $c(n_s)$  for an amplifier with  $n = 2$  (top) and  $n = 3$  (bottom). The horizontal line is the result for constant fraction discrimination at the maximum slope from Eq. 35.

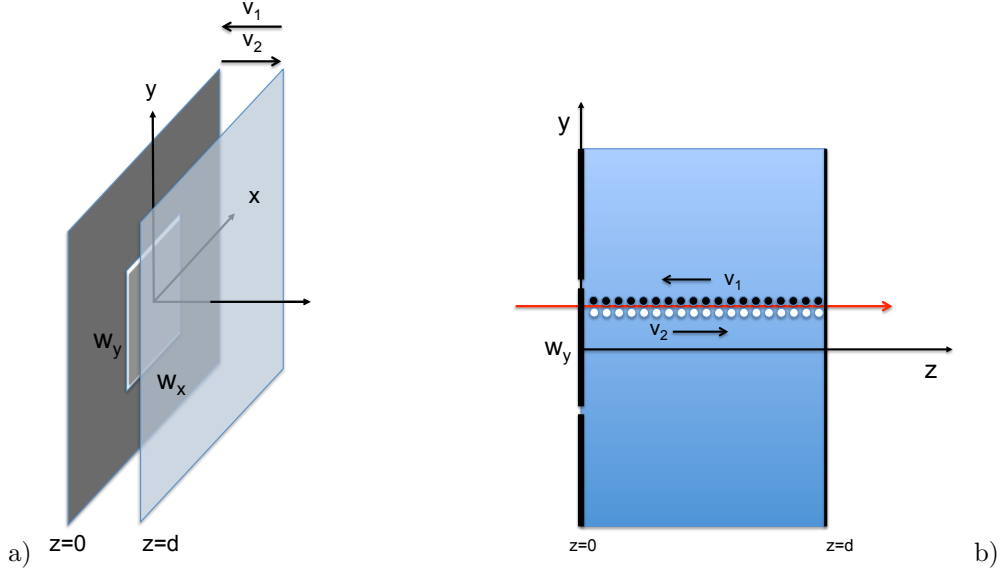


Figure 10: a) A pixel of dimension  $w_x, w_y$  centred at  $x = y = z = 0$  in a parallel plate geometry of plate distance  $d$ . b) Uniform charge deposit of a particle passing the silicon sensor.  $v_1$  is the velocity of charges moving towards the pixel and  $v_2$  is the velocity of charges moving away from the pixel.

#### 4.4. Weighting field effect on the centroid time for uniform charge deposit

Up to now we have assumed the sensor readout electrode to be represented by an infinite parallel plate capacitor, which in practice corresponds to readout pads or pixels that are much larger than the sensor thickness  $d$ . In many practical applications, the granularity is however similar to the sensor thickness. The shape of the induced signal therefore becomes dependent on the  $x, y$  position of the track and the centroid time will be affected. In this section we investigate this effect by using the weighting field of a rectangular pixel as presented in [25], shown in Fig. 10a and detailed in Appendix E.

We assume again the sensor to be represented by a parallel plate geometry between  $z = 0$  and  $z = d$  and assume charges to move along the  $z$ -axis. We also assume normal incidence of the particle and negligible diffusion. The plate at  $z = 0$  is segmented into pixels such that we find a weighting field of  $E_w(x, y, z) = -d\phi_w(x, y, z)/dz$  along the  $z$ -axis. We first assume a single charge pair to be produced at position  $x, y, z$  with  $-q$  moving towards the the pixel at  $z = 0$  according to  $z_1(t) = z - v_1 t$  and  $+q$  moving towards the plate at  $z = d$  according  $z_2(t) = z + v_2 t$ , so the induced current becomes

$$\frac{i(t)}{q} = E_w[x, y, z_1(t)]\dot{z}_1(t)\Theta(z/v_1 - t) + E_w[x, y, z_2(t)]\dot{z}_2(t)\Theta((d - z)/v_2 - t) \quad (49)$$

$$= -v_1 E_w[x, y, z - v_1 t]\Theta(z/v_1 - t) - v_2 E_w[x, y, z + v_2 t]\Theta((d - z)/v_2 - t) \quad (50)$$

The centroid time of this signal is

$$\tau(x, y, z) = \frac{\int t i(t) dt}{\int i(t) dt} = \frac{d}{v_1} \Psi_1(x, y, z) + \frac{d}{v_2} \Psi_2(x, y, z) \quad (51)$$

$$\Psi_1(x, y, z) = \frac{z}{d} - \frac{1}{d} \int_0^z \phi_w(x, y, z') dz' \quad \Psi_2(x, y, z) = \frac{1}{d} \int_z^d \phi_w(x, y, z') dz' \quad (52)$$



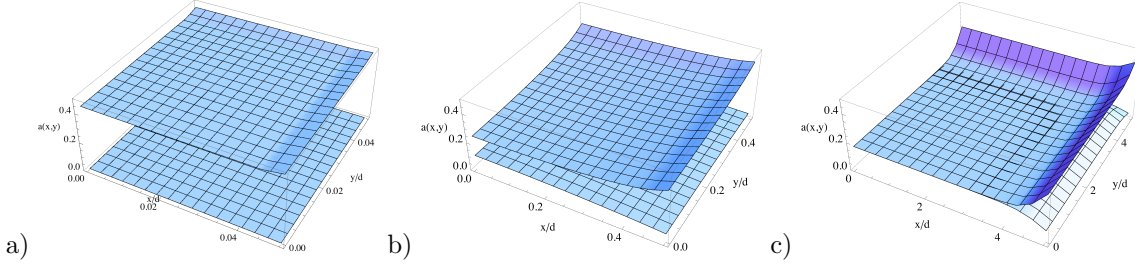


Figure 11: The functions  $a_1(x, y)$  and  $a_2(x, y)$  from Eq. 54 that determine the centroid time for a signal from two line charges  $-q_{line}, q_{line}$  at position  $x, y$ . The top graph corresponds to  $a_1$  and the bottom one to  $a_2$ . The three plots correspond to pads of size a)  $w/d = 0.1$ , b)  $w/d = 1$ , c)  $w/d = 10$ .

In case there is not a single pair of charges  $q, -q$  but a pair of uniform line charges between  $z = 0$  and  $z = d$ , as shown in Fig. 10b, we have

$$\begin{aligned} \frac{I(x, y, t)}{q_{line}} &= -v_1 \int_0^d E_w[x, y, z - v_1 t] \Theta(z/v_1 - t) dz - v_2 \int_0^d E_w[x, y, z + v_2 t] \Theta((d - z)/v_2 - t) dz \\ &= -v_1 [1 - \phi_w(x, y, d - v_1 t)] \Theta(d/v_1 - t) - v_2 \phi_w(x, y, v_2 t) \Theta(d/v_2 - t) \end{aligned} \quad (53)$$

where  $q_{line}$  is the charge per unit of length. The centroid time of this signal then reads as

$$\tau(x, y) = \frac{d}{v_1} a_1(x, y) + \frac{d}{v_2} a_2(x, y) = T_1 a_1(x, y) + T_2 a_2(x, y) \quad (54)$$

$$a_1(x, y) = \frac{1}{d} \int_0^d \Psi_1(x, y, z) dz = \frac{1}{2} - \frac{1}{d^2} \int_0^d (d - z) \phi_w(x, y, z) dz \quad (55)$$

$$a_2(x, y) = \frac{1}{d} \int_0^d \Psi_2(x, y, z) dz = \frac{1}{d^2} \int_0^d z \phi_w(x, y, z) dz \quad (56)$$

The two functions  $a_1(x, y)$  and  $a_2(x, y)$  are shown in Fig. 11. We can see that for large pads the values for both functions approach the constant value of  $1/6$  in accordance with Eq. B.5 with some deviations at the border. For small pads the average of  $a_1$  and  $a_2$  is quite different, but the functions are also quite uniform. For the pad size of  $w/d \approx 1$  the two functions vary significantly across the pad, which we will quantify next. In case the pixel is uniformly irradiated, the probability to hit an area  $dx dy$  is given by  $dx dy/(w_x w_y)$  and the average centroid time, the second moment and the standard deviation  $\Delta_\tau$  are given by

$$\bar{\tau} = \frac{1}{w_x w_y} \int_{-w_x/2}^{w_x/2} \int_{-w_y/2}^{w_y/2} \tau(x, y) dx dy \quad \overline{\tau^2} = \frac{1}{w_x w_y} \int_{-w_x/2}^{w_x/2} \int_{-w_y/2}^{w_y/2} \tau^2(x, y) dx dy \quad (57)$$

$$\Delta_\tau^2 = \overline{\tau^2} - \bar{\tau}^2 = d^2 \left( \frac{c_{11}}{v_1^2} + \frac{c_{12}}{v_1 v_2} + \frac{c_{22}}{v_2^2} \right) = c_{11} T_1^2 + c_{12} T_{12} + c_{22} T_2^2 \quad (58)$$

where we have defined

$$c_{11} = \frac{1}{w_x w_y} \iint a_1^2 dx dy - \left( \frac{1}{w_x w_y} \iint a_1 dx dy \right)^2 \quad (59)$$

$$c_{12} = \frac{2}{w_x w_y} \iint a_1 a_2 dx dy - \frac{2}{(w_x w_y)^2} \iint a_1 dx dy \iint a_2 dx dy \quad (60)$$

$$c_{22} = \frac{1}{w_x w_y} \iint a_2^2 dx dy - \left( \frac{1}{w_x w_y} \iint a_2 dx dy \right)^2 \quad (61)$$

and

$$T_1 = d/v_1 \quad T_2 = d/v_2 \quad T_{12} = d/\sqrt{v_1 v_2} \quad (62)$$

Before moving to the numerical evaluation we investigate the limiting cases for very large and very small pads. For large pixels we have  $\phi_w = 1 - z/d$  and the expressions become

$$a_1(x, y) = \frac{1}{6} \quad a_2(x, y) = \frac{1}{6} \quad \text{for} \quad w/d \gg 1 \quad (63)$$

which results in  $\bar{\tau} = d/6(1/v_1 + 1/v_2)$  in accordance with Eq. B.5 for an infinite electrode. Since there is no dependence on  $x$  and  $y$ , the coefficients  $c_{11}, c_{12}, c_{22}$  vanish, which is the expected result for an infinitely electrode.

For very small pads the weighting potential falls to zero very quickly as a function of  $z$ , from it's value of unity on the pad surface at  $z = 0$ . The integrals of the weighting potential over  $z$  will therefore vanish and we have

$$a_1(x, y) = \frac{1}{2} \quad a_2(x, y) = 0 \quad \text{for} \quad w/d \ll 1 \quad (64)$$

For this case only the charges moving towards the pad with  $v_1$  contribute to the centroid time and the average centroid time becomes  $\bar{\tau} = d/2v_1$ . Since the weighting potential and weighting field are concentrated around the pixel surface the charges that never enter this area, i.e. the charges moving with  $v_2$  towards  $z = d$  will not contribute to the signal. The coefficients  $c_{11}, c_{12}, c_{22}$  will again vanish because  $a_1$  and  $a_2$  have no dependence on  $x, y$ . Because the two limiting cases are zero, this means that there will be a pad size where the effect of the weighting field fluctuation is maximal, as discussed in the following.

The numerical evaluation of Eqs. 59, 60, 61 for square pixels of width  $w$  for different ratios of  $w/d$  are given in Table E.1 of the Appendix and the graphical representation of the coefficients is shown in Fig. 12. The weighting potential of a pixel as given in Eq. E.1 of the Appendix is used. The weighting field effect on the time resolution is worst for pad sizes corresponding to about 2-3 times the sensor thickness  $d$ , where the  $c_{11}$  and  $c_{12}$  coefficients assume a value around  $2 \times 10^{-3}$ . The coefficient  $c_{11}$  is related to  $v_1$  i.e. to the charges moving to the readout pad,  $c_{22}$  is related to the charges moving in opposite direction. Since  $c_{11} > c_{22}$  by a significant factor, the time resolution will be better if  $v_1 > v_2$  i.e. if the electrons are moving towards the pixels. The contribution to the time resolution from Eq. 58 is shown in Fig. 13. In case the holes move towards the pixel we find a maximum for values of  $w/d \approx 2$ , where the contribution becomes similar to the value from Landau fluctuations. In case the electrons move towards the pixel, the contribution is significantly smaller with maxima around  $w/d \approx 1$ .

The somewhat slow decrease of the effect for pad sizes of  $w/d > 3$  is due to the fact that we are calculating the standard deviation of the centroid time. As shown in Fig. 11c) for  $w/d = 10$  there is no variation of the centroid time in the central 70% of the pixel area and the variations take place only at the edges. The resulting time distribution for uniform illumination is significantly non-Gaussian with long tails. The true impact on the time resolution therefore depends also on the method of using the measured time and the algorithm for defining the time resolution.

The final resolution is not given by the square sum of the Landau fluctuations from Eq. 20 and the weighting field fluctuations from Eq. 58, since there is a very strong correlation between the two. This will be discussed in the next section.

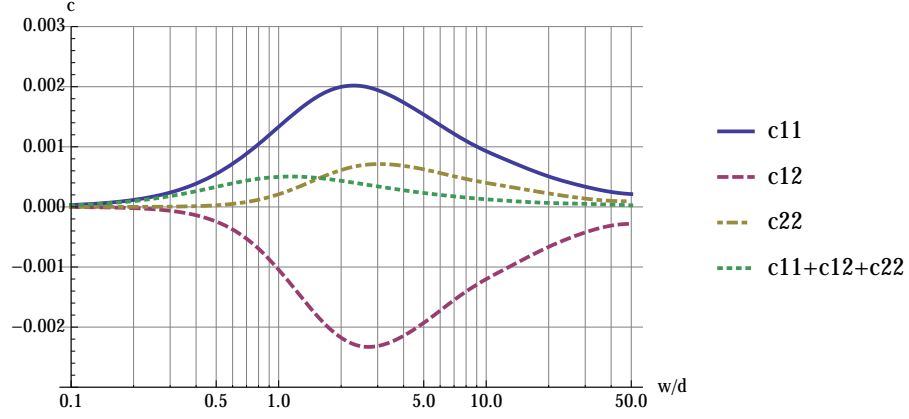


Figure 12: The coefficients  $c_{11}, c_{12}, c_{22}$  for different values of  $w/d$ , where  $w$  is the width of the square pad and  $d$  is the silicon sensor thickness.

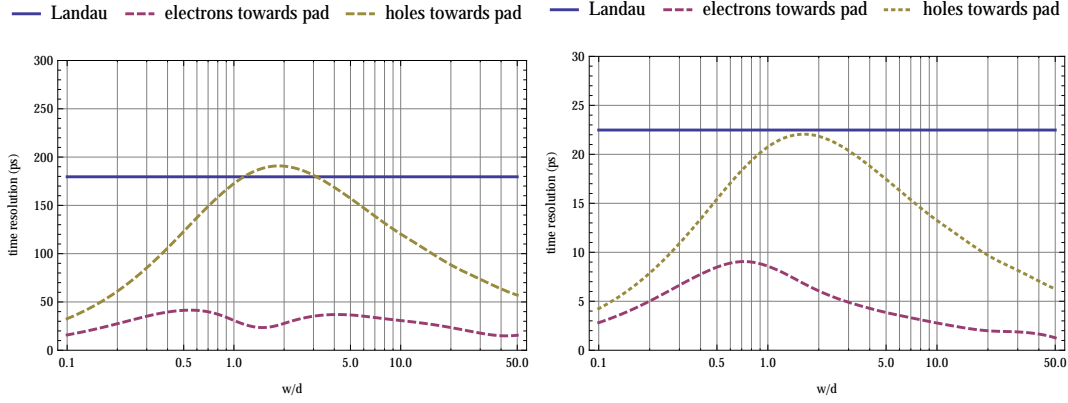


Figure 13: Standard deviation for the centroid time for sensor thickness of a)  $d = 200 \mu\text{m}$  and b)  $d = 50 \mu\text{m}$  and  $V = 200 \text{ V}$ , assuming uniform charge deposit and a square readout pad. The horizontal line represents centroid time resolution from Eq. 20 due to Landau fluctuations only. The two curves in the plots represent the effect of weighting field fluctuations where either the electrons or the holes move towards the readout pad.

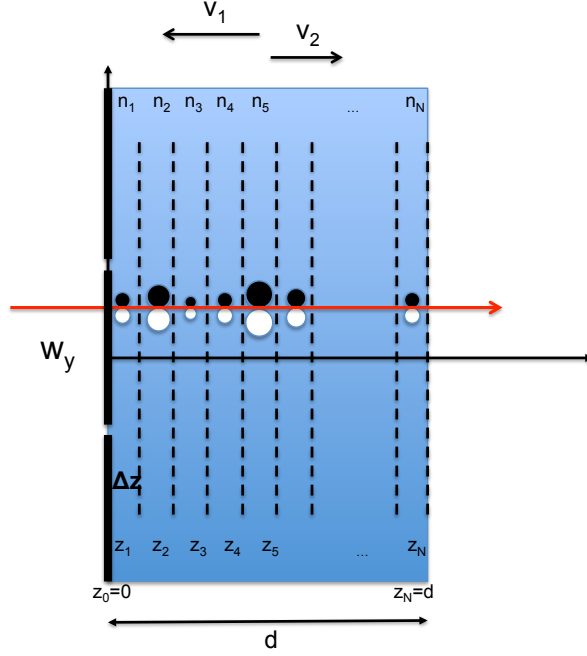


Figure 14: Silicon sensor with a readout pad centered at  $x = y = z = 0$ .  $v_1$  is the velocity of charges moving towards the pixel and  $v_2$  is the velocity of charges moving away from the pixel.

#### 4.5. Centroid time resolution for combined charge fluctuations and weighting field fluctuations

In this section we consider the Landau fluctuations together with the variation of the  $x, y$  position of the particle trajectory and the related fluctuation of the weighting field. The centroid time for a particle that passes the sensor at position  $x, y$  and deposits  $n_k$  charges in the  $N$  detector slices is given by

$$\tau(n_1, n_2, \dots, n_N, x, y) = \frac{1}{\sum_{k=1}^N n_k} \sum_{k=1}^N n_k \tau(x, y, k\Delta z) \quad (65)$$

where  $\tau(x, y, z)$  is from Eq. 51. Proceeding as detailed in Appendix B we calculate  $\bar{\tau}$  and  $\overline{\tau^2}$ , where in addition to the integrals over  $dn_1, dn_2, \dots, dn_N$  we have to perform the integral  $1/(w_x w_y) \int \int \tau dx dy$  for uniform illumination of a pad, and the final result for the variance is

$$\begin{aligned} \overline{\tau^2} - \bar{\tau}^2 &= w(d)^2 \frac{1}{w_x w_y} \iint \left[ \frac{1}{d} \int_0^d \tau(x, y, z)^2 dz - \left( \frac{1}{d} \int_0^d \tau(x, y, z) dz \right)^2 \right] dx dy \\ &+ \frac{1}{w_x w_y} \iint \left( \frac{1}{d} \int_0^d \tau(x, y, z) dz \right)^2 dx dy - \left[ \frac{1}{w_x w_y} \iint \left( \frac{1}{d} \int_0^d \tau(x, y, z) dz \right) dx dy \right]^2 \end{aligned} \quad (66)$$

The second line of the expression is equivalent to the one considering the weighting field effect without charge fluctuations from the previous section, so the result can be expressed in the following terms

$$\Delta_\tau^2 = w(d)^2 \left( \frac{k_{11} d^2}{v_1^2} + \frac{k_{12} d^2}{v_1 v_2} + \frac{k_{22} d^2}{v_2^2} \right) + \left( \frac{c_{11} d^2}{v_1^2} + \frac{c_{12} d^2}{v_1 v_2} + \frac{c_{22} d^2}{v_2^2} \right) \quad (67)$$

The coefficients  $c_{11}, c_{12}, c_{22}$  are the ones from the previous section and the coefficients  $k_{11}, k_{12}, k_{22}$  are given by

$$k_{11} = \frac{1}{w_x w_y} \iint (b_{11} - a_1^2) dx dy \quad k_{12} = \frac{2}{w_x w_y} \iint (b_{12} - a_1 a_2) dx dy \quad k_{22} = \frac{1}{w_x w_y} \iint (b_{22} - a_2^2) dx dy \quad (68)$$

with

$$\begin{aligned} b_{11}(x, y) &= \frac{1}{d} \int_0^d \Psi_1(x, y, z)^2 dz = \frac{1}{d} \int_0^d \left[ \frac{z}{d} - \frac{1}{d} \int_0^z \phi_w(x, y, z') dz' \right]^2 dz \\ b_{12}(x, y) &= \frac{1}{d} \int_0^d \Psi_1(x, y, z) \Psi_2(x, y, z) dz = \frac{1}{d} \int_0^d \left[ \frac{z}{d} - \frac{1}{d} \int_0^z \phi_w(x, y, z') dz' \right] \left[ \frac{1}{d} \int_z^d \phi_w(x, y, z') dz' \right] dz \\ b_{22}(x, y) &= \frac{1}{d} \int_0^d \Psi_2(x, y, z)^2 dz = \frac{1}{d} \int_0^d \left[ \frac{1}{d} \int_z^d \phi_w(x, y, z') dz' \right]^2 dz \end{aligned} \quad (69)$$

First we verify the limiting cases for very large pads and very small pads. For large pads we substitute for the weighting potential the expression  $\phi_w(x, y, z) = 1 - z/d$  and find

$$b_{11}(x, y) = \frac{1}{20} \quad b_{12}(x, y) = \frac{1}{120} \quad b_{22}(x, y) = \frac{1}{20} \quad w/d \gg 1 \quad (70)$$

which gives  $k_{11} = k_{22} = 4/180, k_{12} = -7/180$  and  $c_{11} = c_{12} = c_{22} = 0$ , so we recuperate Eq. B.19. For very small pads the integrals of the weighting potential over  $z$  will again vanish as discussed before, and we have

$$b_{11}(x, y) = \frac{1}{3} \quad b_{12}(x, y) = 0 \quad b_{22}(x, y) = 0 \quad w/d \ll 1 \quad (71)$$

which gives  $k_{11} = 1/12, k_{12} = k_{22} = 0$  and  $c_{11} = c_{12} = c_{22} = 0$  and therefore have

$$\Delta_\tau = w(d) \frac{T_1}{\sqrt{12}} \quad (72)$$

For small pads the weighting potential decays very quickly as a function of  $z$ , from its value of 1 on the pad surface to zero. The weighting field, which defines the induced current, is therefore very large close to the pad and zero for larger values of  $z$ . Only when the charges arrive at this position they will induce a signal. In the limiting case this is equivalent to a delta current signal for each charge that arrives at  $z = 0$ , and we have

$$i(t) = q \sum_{k=1}^N n_k \delta(t - k\Delta z/v_1) \quad \tau = \frac{1}{\sum_{k=1}^N n_k} \sum_{k=1}^N n_k k\Delta z/v_1 \quad \Delta_\tau = w(d) \frac{T_1}{\sqrt{12}} \quad (73)$$

so we indeed recuperate the above expression for  $\Delta_\tau$  ! We'll see the same formula later in Eq. 90 for silicon sensors with gain.

The coefficients  $k_{11}, k_{12}, k_{22}$  for square pads are listed in Table E.2 of the Appendix and are shown in Fig. 15. The factor  $k_{11}$ , related to the charges moving with  $v_1$  towards the pixel, is again larger than  $k_{22}$ , so as stated before the resolution is better if the electrons move towards the pixel. This fact is illustrated in Fig. 16 and Fig. 17 for a  $200 \mu\text{m}$  and  $50 \mu\text{m}$  sensor. It shows a significant difference for these two scenarios. In case the electrons move to the pixel the weighting field effect seems not to add significantly to the time resolution for values of  $w/d \gtrsim 1$ .

For pads with  $w/d > 20$  one approaches the scenario of an infinitely extended electrode, as expected. For smaller pixels the Landau fluctuations and weighting field effect are strongly correlated and the resolution is significantly worse than expected from the quadratic sum of the weighting field effect for uniform charge deposit and the Landau fluctuation effects assuming an infinitely large electrode.

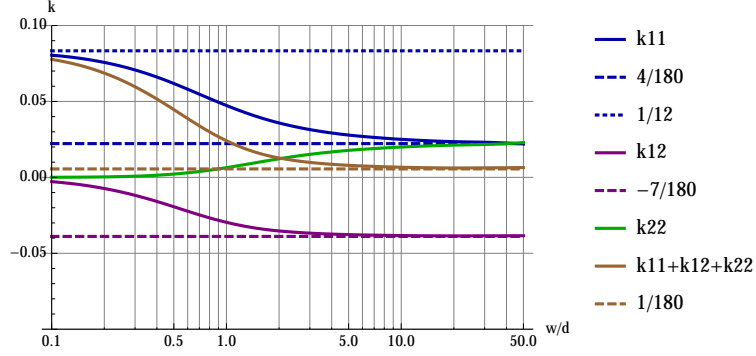


Figure 15: The coefficients  $k_{11}, k_{12}, k_{22}$  for different values of  $w/d$ , where  $w$  is the width of the square pad and  $d$  is the silicon thickness. The dotted lines represent the for very small pads and very large pads as discussed in the text.

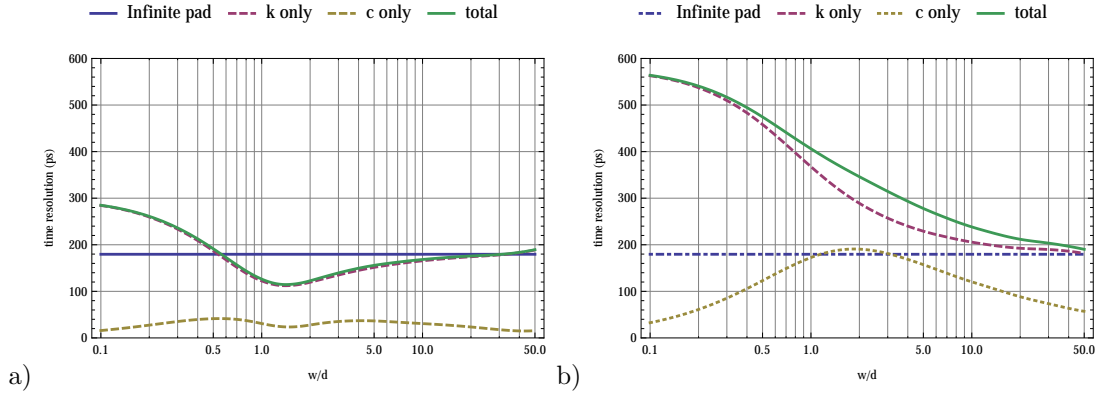


Figure 16: Centroid time resolution for values of  $d = 200 \mu\text{m}$  and  $V = 200 \text{ V}$  as a function of the pixel size  $w$  assuming the Landau theory for the charge deposit. The 'c only' curve refers to the effect from a uniform line charge. In a) the electrons move towards the pixel while in b) the holes move towards the pixel.

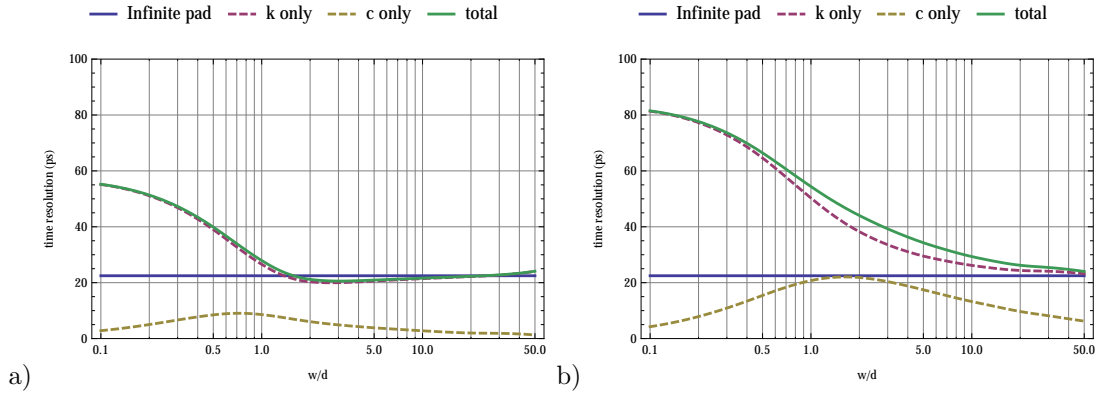


Figure 17: Time resolution for values of  $d = 50 \mu\text{m}$  and  $V = 200 \text{ V}$  as a function of the pixel size  $w$  assuming the Landau theory for the charge deposit. The 'c only' curve refers to the effect from a uniform line charge. In a) the electrons move towards the pixel while in b) the holes move towards the pixel.

#### 4.6. Leading edge discrimination

Up to this point we have just discussed the centroid time of the detector signals. In this section we consider the measured time to be determined by leading edge discrimination of the normalized detector signal. We process the detector signal by an amplifier of a given peaking time, and perform the so called 'slewing correction' for eliminating the timewalk effect from pulseheight fluctuations by dividing the amplifier output signal by the total signal charge and set the threshold to a given fraction of this signal. The current signal due to a single charge pair  $-q, q$  at position  $x, y, z$  is

$$i_0(x, y, z, t) = -q [v_1 E_w(x, y, z - v_1 t) \Theta(z/v_1 - t) + v_2 E_w(x, y, z + v_2 t) \Theta((d - z)/v_2 - t)] \quad (74)$$

The current signal for having  $n_1$  e/h pairs at  $z = \Delta z$ ,  $n_2$  e/h pairs at  $z = 2\Delta z$  etc. is given by

$$i(n_1, n_2, \dots, n_N, x, y, t) = \sum_{k=1}^N n_k i_0(x, y, k\Delta z, t) \quad (75)$$

We now process this signal by an amplifier with delta response  $cf(t/t_p)$  where  $t_p$  is the peaking time,  $f(1) = 1$ ,  $c$  is the amplifier sensitivity in units of  $[V/C]$  and  $f(x)$  is defined by

$$f(x) = x^n e^{n(1-x)} \quad (76)$$

The amplifier output signal is the given by the convolution of the induced signal and the amplifier delta response

$$s(n_1, n_2, \dots, n_N, x, y, t) = c \int_0^t f\left(\frac{t-t'}{t_p}\right) i(n_1, n_2, \dots, n_N, x, y, t') dt' \quad (77)$$

$$= c q \sum_{k=1}^N n_k g(x, y, k\Delta z, t) \quad (78)$$

where  $g(x, y, z, t)$  is

$$\begin{aligned} g(x, y, z, t) &= \Theta(z - v_1 t) \int_{\frac{z-v_1 t}{d}}^{\frac{z}{d}} f\left(\frac{v_1 t - z + ud}{v_1 t_p}\right) E_w^z(x/d, y/d, u, w_x/d, w_y/d, 1) du \\ &+ \Theta(v_1 t - z) \int_0^{\frac{z}{d}} f\left(\frac{v_1 t - z + ud}{v_1 t_p}\right) E_w^z(x/d, y/d, u, w_x/d, w_y/d, 1) du \\ &+ \Theta[(d - z) - v_2 t] \int_{\frac{z}{d}}^{\frac{z+v_2 t}{d}} f\left(\frac{v_2 t + z - ud}{v_2 t_p}\right) E_w^z(x/d, y/d, u, w_x/d, w_y/d, 1) du \\ &+ \Theta[v_2 t - (d - z)] \int_{\frac{z}{d}}^1 f\left(\frac{v_2 t + z - ud}{v_2 t_p}\right) E_w^z(x/d, y/d, u, w_x/d, w_y/d, 1) du \end{aligned} \quad (79)$$

The weighting field  $E_w^z(x, y, z, w_x, w_y, d)$  for a pixel is given in Eq. E.6 of Appendix E. To perform slewing corrections we divide the signal by the total charge  $q \sum n_k$  and we get the normalized amplifier output signal

$$h(n_1, n_2, \dots, n_N, x, y, t) = \frac{c}{\sum_{k=1}^N n_k} \sum_{k=1}^N n_k g(x, y, k\Delta z, t) \quad (80)$$

The average normalized signal and the variance of the signal evaluate to

$$\bar{h}(t) = \frac{c}{w_x w_y} \iint \left[ \int_0^1 g(x, y, sd, t) ds \right] dx dy \quad (81)$$

and

$$\begin{aligned}\Delta_h^2(t) &= w(d)^2 \frac{c^2}{w_x w_y} \iint \left[ \int_0^1 g(x, y, sd, t)^2 ds - \left( \int_0^1 g(x, y, sd, t) ds \right)^2 \right] dx dy \\ &+ \frac{c^2}{w_x w_y} \iint \left( \int_0^1 g(x, y, sd, t) ds \right)^2 dx dy - \left[ \frac{c}{w_x w_y} \iint \left( \int_0^1 g(x, y, sd, t) ds \right) dx dy \right]^2\end{aligned}\quad (82)$$

The time resolution is then defined by (Fig. 18b)

$$\sigma_t = \frac{\Delta_h(t)}{\overline{h}'(t)} \quad (83)$$

Here we just discuss the example of an infinitely extended pixel i.e. we use  $E_w^z(x, y, z, w_x, w_y, d) = 1/d$ , which evaluates  $g(x, y, z, t)$  to

$$\begin{aligned}\frac{n^{n+1}}{e^n} \frac{d}{t_p} g(x, y, z, t) &= v_1 \Theta(z - v_1 t) [n! - \Gamma(n+1, t/t_p)] \\ &- v_1 \Theta(v_1 t - z) [\Gamma(n+1, t/t_p) - \Gamma(n+1, -(z - v_1 t)/(t_p v_1))] \\ &+ v_2 \Theta((d - z) - v_2 t) [n! - \Gamma(n+1, t/t_p)] \\ &- v_2 \Theta(v_2 t - (d - z)) [\Gamma(n+1, t/t_p) - \Gamma(n+1, -(d - z - v_2 t)/(t_p v_2))]\end{aligned}$$

where  $n$  and  $t_p$  are the parameters defining the amplifier. As an example the average signal  $\bar{h}(t)$  for a  $50 \mu\text{m}$  sensor at 200 V for different peaking times is shown in Fig. 18a. The signal duration is around 0.8 ns, so for small peaking times of 0.25 and 0.5 ns there is significant 'ballistic deficit' while for peaking times  $> 1$  ns the amplifier 'integrates' the full signal and the normalized amplitude becomes unity. In Fig. 18b the average normalized signal for a peaking time of 0.25 ns is shown, together with  $\pm 1$  standard deviations.

The resulting time resolution is shown in Fig. 19a and Fig. 20a for a  $50 \mu\text{m}$  and a  $200 \mu\text{m}$  sensor. We find that for large peaking times, the time resolution indeed approaches the centroid time value, while for smaller peaking times the time resolution can be significantly better when setting the threshold at less than 30-40% of the normalized signal. E.g. for the  $50 \mu\text{m}$  sensor at 200 V, a peaking time of 0.25 ns and a threshold set to 40% of the total signal charge one should arrive at a resolution that is two times better than the resolution achieved with the centroid time. For a  $200 \mu\text{m}$  sensor,  $t_p = 5$  ns and a threshold at 30% of the signal one also expects a twice better resolution as compared to the centroid time.

To study the impact of the noise we assume  $\sigma_{noise}$  to be given in units of electrons. This noise is superimposed to the signal  $s(t)$  from Eq. 77, so when normalizing the signal to arrive at  $h(t)$  we also have to normalize the noise by the total amount of charge deposited in the sensor. The average normalized noise then becomes

$$\bar{\sigma}_{norm} = \int_0^\infty \frac{\sigma_{noise}}{n} p(n, d) dn = \sigma_{noise} \frac{\lambda}{n_0 d} \frac{1}{1 + 1.155 \ln d/\lambda} \quad (84)$$

The contribution of the noise to the time resolution is then

$$\sigma_t = \frac{\bar{\sigma}_{norm}}{\overline{h}'(t)} \quad (85)$$

We can therefore express the required noise level when using a threshold of  $\bar{h}(t)$ , that matches the resolution from Landau fluctuations from Eq. 83, as

$$\sigma_{noise} [electrons] = \Delta_h(t) \frac{n_0 d}{\lambda} (1 + 1.155 \ln d/\lambda) \quad (86)$$

The numbers are shown in Fig. 19b and Fig. 20b. For the  $50 \mu\text{m}$  sensor and  $t_p = 0.25$  ns the required noise level is 100 electrons and for the  $200 \mu\text{m}$  sensor at  $t_p = 5$  ns the required noise is 400 electrons.



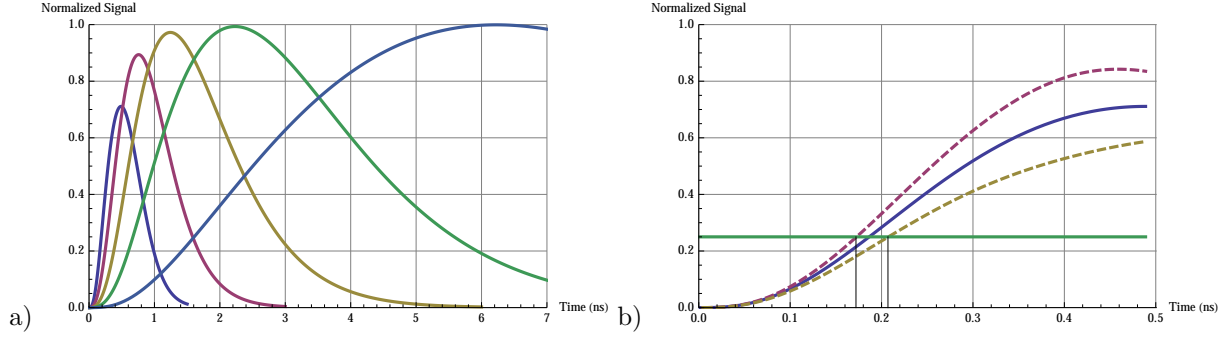


Figure 18: a) Average normalized signal  $\bar{h}(t)$  for amplifier peaking times  $t_p = 0.25, 0.5, 1, 2, 6$  ns for a  $50\mu\text{m}$  sensor and  $V=200$  V. b) Average normalized signal  $\bar{h}(t)$  for  $t_p = 0.25$  ns together with the curves  $\bar{h}(t) + \Delta_h(t)$  and  $\bar{h}(t) - \Delta_h(t)$ .

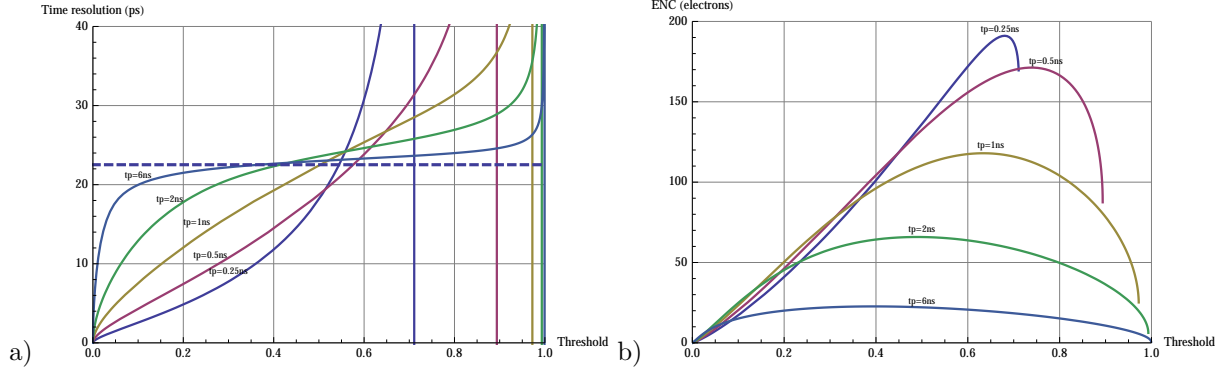


Figure 19: a) Time resolution for a sensor of  $50\mu\text{m}$  thickness at 200 V bias voltage. The slewing correction is performed by dividing the signal by the total charge and applying the threshold as a fraction of this charge. b) ENC needed to match the noise contribution to the effect from the Landau fluctuations.

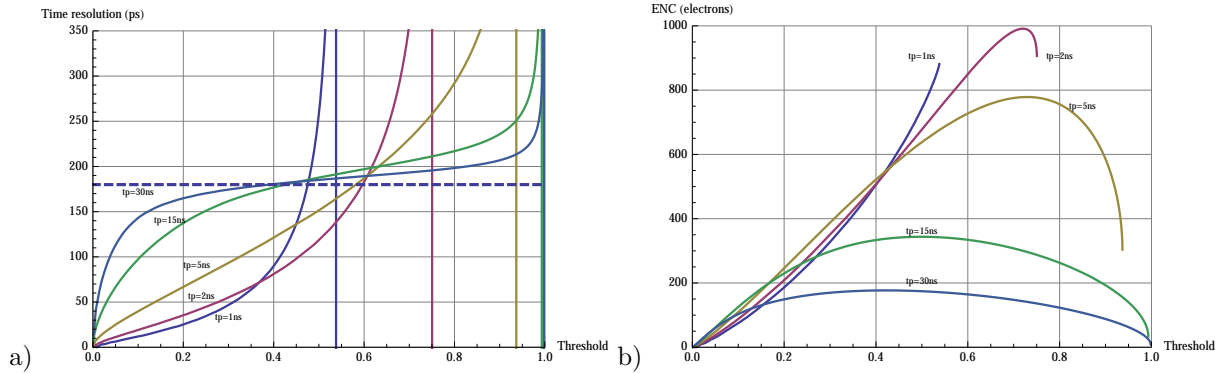


Figure 20: a) Time resolution for a sensor of  $200\mu\text{m}$  thickness at 200 V bias voltage. The slewing correction is performed by dividing the signal by the total charge and applying the threshold as a fraction of this charge. b) ENC needed to match the noise contribution to the effect from the Landau fluctuations.

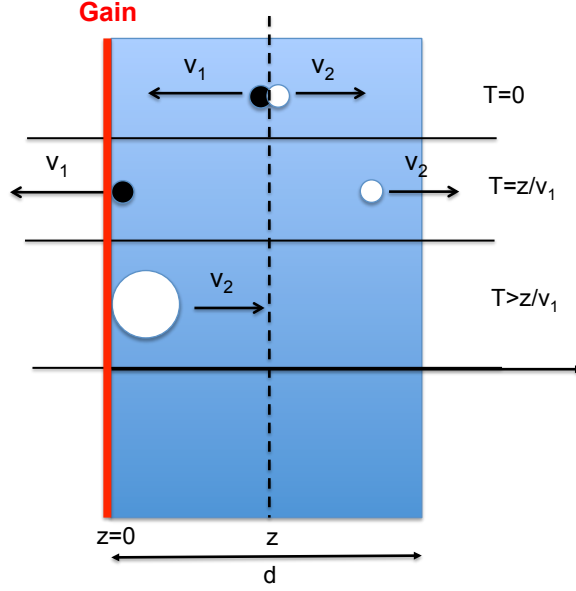


Figure 21: Silicon sensor with internal gain. An e-h par is produced at position  $z$ , the electron arrives at  $z = 0$  at time  $T = z/v_1$ , the electron multiplies in a high field layer at  $z = 0$  and the holes move back to  $z = d$ , inducing the dominant part of the current signal.

## 5. Silicon sensors with internal gain

### 5.1. Centroid time resolution for silicon sensors with internal gain

In the Low Gain Avalanche Diode (LGAD), a high field region is implemented in the sensor in order to multiply electrons at some moderate gain and as a result improve the signal to noise ratio. We assume the geometry from Fig. 21 with the amplification structure located at  $z = 0$ . The electrons will therefore move from their point of creation to this structure, get multiplied and the holes created in the multiplication process are moving back from  $z = 0$  to  $z = d$  through the entire sensor thickness  $d$ . If we assume 1) the gain  $G$  to be sufficiently large such that the signal from the primary electron and hole movement is negligible, 2) the amplification structure to be infinitely thin, 3) a sensor with negligible depletion voltage, the signal from a single e-h pair created at position  $z$  is of rectangular shape with duration  $T = d/v_2$ , shifted by the time  $t = z/v_1$

$$i(t) = -G \frac{q v_2}{d} [\Theta(t - z/v_1) - \Theta(t - z/v_1 - d/v_2)] \quad (87)$$

The centroid time of this signal is

$$\tau = \frac{d}{2v_2} + \frac{z}{v_1} \quad (88)$$

The centroid time for the case of  $n_1, n_2, \dots, n_N$  clusters at positions  $z_1, z_2, \dots, z_N$  is

$$\tau(n_1, n_2, \dots, n_N) = \frac{1}{\sum_{k=1}^N n_k} \sum_{k=1}^N n_k \left( \frac{d}{2v_2} + \frac{z_k}{v_1} \right) = \frac{d}{2v_2} + \frac{1}{\sum_{k=1}^N n_k} \sum_{k=1}^N n_k \frac{z_k}{v_1} \quad (89)$$

The average and standard deviation of the centroid time are then

$$\bar{\tau} = \frac{d}{2} \left( \frac{1}{v_1} + \frac{1}{v_2} \right) \quad \Delta\tau = w(d) \frac{d}{\sqrt{12}v_1} \approx \frac{1}{\sqrt{a + b \ln d/\lambda + c(\ln d/\lambda)^2}} \frac{T_1}{\sqrt{12}} \quad (90)$$

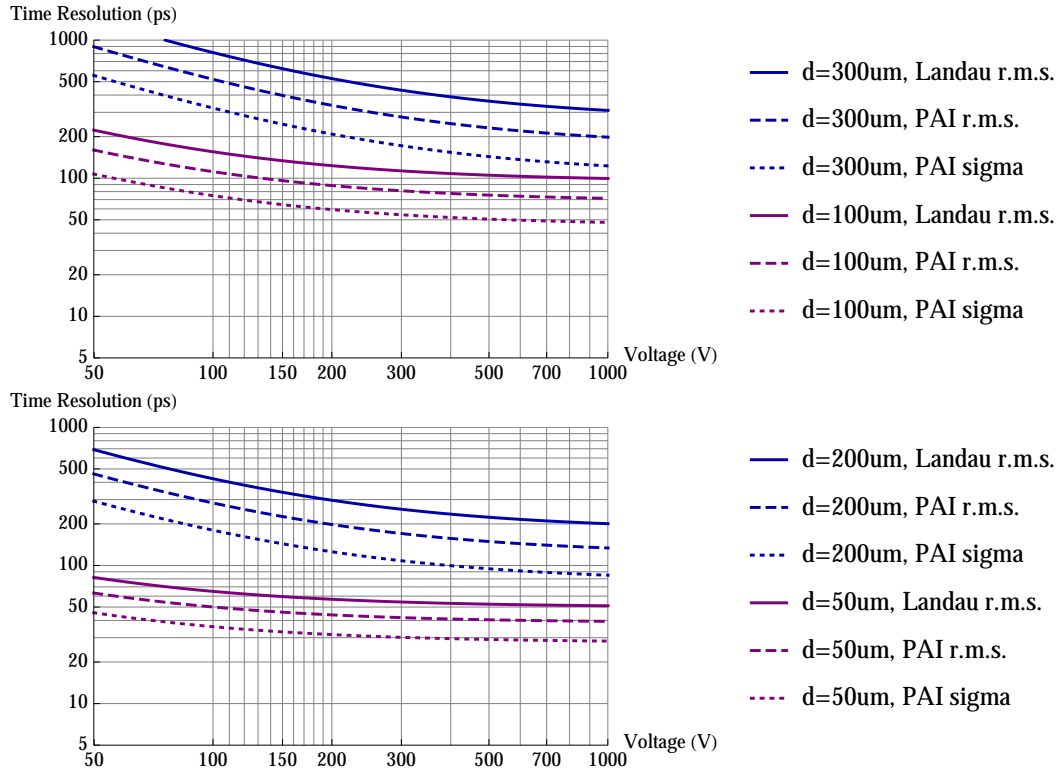


Figure 22: Time resolution for the centroid time from Eq. 90 for 50, 100, 200, 300  $\mu\text{m}$  silicon sensors with internal gain of electrons, assuming a signal only from gain holes. The three curves for each sensor thickness correspond to the Landau theory, the PAI model and a Gaussian fit to the PAI model.

with  $T_1 = d/v_1$  being the total electron drift time. This expression is the same as the one from Eq. 72 and Eq. 73, so this sensor is simply measuring the arrival time distribution of the electrons at  $z = 0$ . The resulting time resolution for 50, 100, 200, 300  $\mu\text{m}$  sensors is shown in Fig. 22. Although the time resolution for the sensors with gain is worse than the one for silicon sensors without gain as shown in Fig. 6, the big advantage of the sensors with gain is the improved signal to noise ratio that can 'eliminate' the effect from the noise. For a 50  $\mu\text{m}$  sensor at 220 V one can achieve a time resolution of 30 ps in accordance with measurements on the LGAD sensors.

The effects defining the time resolution for a sensor with gain therefore differ significantly from one without gain. The electrons first have to arrive at  $z = 0$  before being amplified and producing the gain signal, so the signal timing is defined by the arrival time distribution of the electron clusters at  $z = 0$ . This is also illustrated by the fact that the second factor in Eq. 90 is simply the total transit time  $T_e = d/v_1$  of the electrons through the full silicon thickness divided by  $\sqrt{12}$ .

### 5.2. Weighting field effect on the centroid time for silicon sensors with gain

In this section we discuss the effect of the finite pixel size on the centroid time resolution for sensors with gain. Assuming the readout electrode at  $z = 0$  to be segmented into pixels with an associated weighting potential  $\phi_w(x, y, z)$ , the induced signal due to a single charge pair created at position  $x, y, z$  at  $t = 0$  becomes

$$i(t) = -Gq v_2 E_w[x, y, v_2(t - z/v_1)] [\Theta(t - z/v_1) - \Theta(t - z/v_1 - d/v_2)] \quad (91)$$

and the centroid time for this signal is given by

$$\tau(x, y, z) = \frac{z}{v_1} + \frac{d}{v_2} \int_0^1 \phi_w(x, y, s d) ds \quad (92)$$

Assuming a uniform charge deposit along the track, the centroid time becomes

$$\tau(x, y) = \frac{1}{d} \int_0^d \tau(x, y, z) dz = \frac{d}{2v_1} + \frac{d}{v_2} \int_0^1 \phi_w(x, y, s d) ds \quad (93)$$

The variance for uniform irradiation of the pad is then

$$\begin{aligned} \Delta_\tau^2 &= \overline{\tau^2} - \bar{\tau}^2 \\ &= \frac{d^2}{v_2^2} \left[ \frac{1}{w_x w_y} \iint \left( \int_0^1 \phi_w(x, y, s d) ds \right)^2 dx dy - \left( \frac{1}{w_x w_y} \iint \left( \int_0^1 \phi_w(x, y, s d) ds \right) dx dy \right)^2 \right] \\ &= \frac{d^2}{v_2^2} s_{22} = T_2^2 s_{22} \end{aligned} \quad (94)$$

which is the pendant to Eq. 58 for sensors without gain. The coefficient  $s_{22}$  for different pixel sizes is are listed in Teable E.3 and shown in Fig. 23a. The effect on the time resolution for a 50  $\mu\text{m}$  sensor is shown in Fig. 23b. The effect is again largest for pixel sizes of  $w/d \approx 3$ . In case we also take into account the Landau fluctuations we have to use Eq. 92 in Eq. 66 and find

$$\Delta_\tau^2 = \overline{\tau^2} - \bar{\tau}^2 = w(d)^2 \frac{d^2}{12 v_1^2} + \frac{d^2}{v_2^2} s_{22} = w(d)^2 \frac{T_1^2}{12} + T_2^2 s_{22} \quad (95)$$

which is the pendant to Eq. 67 for sensors without gain. So we find the interesting result that for this case there is no correlation between the Landau fluctuations and the weighting field fluctuations, and the two components just add in squares. We also note that the result will be the same whether we segment the electrode at  $z = 0$  where the multiplication takes place or whether we segment the electrode at  $z = d$ .

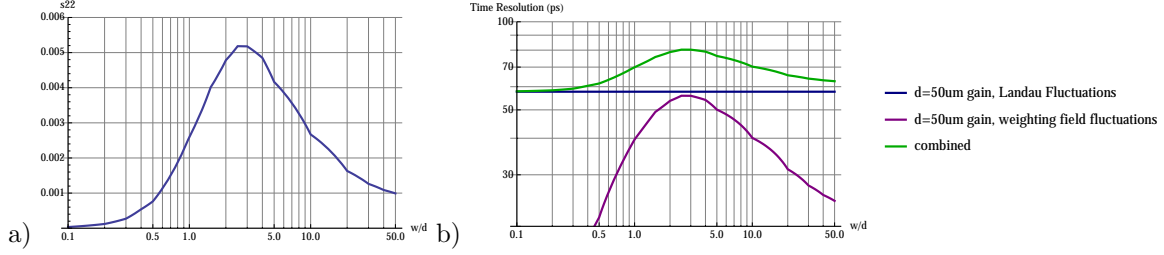


Figure 23: a) Coefficient  $s_{22}$  defining the impact of the weighting field on the time resolution. b) Centroid time resolution for a gain sensor of  $50\text{ }\mu\text{m}$  thickness at 200 V. The horizontal line shows the contribution from Landau fluctuations only, while the other lines show the contribution from weighting field fluctuations as well as the combined effect.

### 5.3. Impact of gain fluctuations

The electron amplification in the gain layer of the LGAD will have statistical fluctuations and in the following we want to quantify the impact of these fluctuations. In case the amplification process is such that the ionizing collisions are independent and do not have a history to the previous collision, the fluctuations of the gain for a single electron are governed by the Yule-Furry law according to

$$p(G) = \frac{1}{\bar{G}} \left(1 - \frac{1}{\bar{G}}\right)^{G-1} \quad \Delta_G^2 = \bar{G}(\bar{G} - 1) \approx \bar{G}^2 \quad (96)$$

where  $\bar{G}$  is the average gain. This assumption is correct as long as the fields are sufficiently low such that there is only electron multiplication and the multiplication of holes is negligible. In case there are  $n \gg 1$  primary electrons, the distribution of the number of electrons after multiplication will assume a Gaussian shape with  $\mu = n\bar{G}$  and  $\sigma^2 = n\Delta_G^2 = n\bar{G}^2$  due to the central limit theorem. The resulting charge spectrum is therefore a convolution of this Gaussian with the Landau distribution  $p(n, d)$ . To estimate the effect of the gain fluctuations on the Landau distribution we approximate the Landau distribution with a Gaussian of mean and standard deviation according to

$$\mu = n_{MP} \quad \sigma = \frac{\Delta n_{FWHM}}{2\sqrt{2\ln 2}} \quad (97)$$

The convolution of this Gaussian with the Gaussian from the gain fluctuations will then again result in a Gaussian where the variances are added in squares and we have

$$\frac{\Delta n_{FWHM}^G}{n_{MP}} = \frac{\Delta n_{FWHM}}{n_{MP}} \sqrt{1 + \frac{n_{MP} 8 \ln 2}{\Delta n_{FWHM}^2}} \approx \frac{\Delta n_{FWHM}}{n_{MP}} \left(1 + \frac{n_{MP} 4 \ln 2}{\Delta n_{FWHM}^2}\right) = \frac{\Delta n_{FWHM}}{n_{MP}} (1 + \varepsilon) \quad (98)$$

The value of  $\varepsilon$  ranges from  $1.9 \times 10^{-3}$  for  $d = 50\text{ }\mu\text{m}$  to  $4.1 \times 10^{-4}$  for  $d = 300\text{ }\mu\text{m}$ . The gain fluctuations will therefore increase the relative fluctuations of the charge deposit by less than 0.2% for a  $50\text{ }\mu\text{m}$  sensor and even less for the  $300\text{ }\mu\text{m}$  sensor.

The correct resulting charge distribution  $p_G(n, d)$  when assuming the Landau distribution  $p(n, d)$  for the primary charge deposit is given by

$$p_G(n, d) = \frac{1}{G} \int_0^\infty p(m, d) \frac{1}{\sqrt{2\pi m}} \exp\left(-\frac{(n/G - m)^2}{2m}\right) dm \quad (99)$$

and the evaluation is shown in Appendix D. The correct values of  $\epsilon$  for the increase of the FWHM with respect to the original distribution are  $2.8/1.6/0.86/0.61 \times 10^{-3}$  for the  $50/100/200/300\text{ }\mu\text{m}$  sensor.

In order to evaluate the impact on the time resolution we have to find the effective cluster size distribution  $p_{clu}^G(n)$ . For large numbers of  $\overline{G}$ , the Furry law turns into the exponential distribution

$$p(G) = \frac{1}{\overline{G}} e^{-G/\overline{G}} \quad (100)$$

Even for the typically low LGAD gains of about 20 this is a good approximation. The probability to find  $n$  electrons for  $m$  primary electrons is then given by the  $n$ -times self convolution of this expression and we have

$$p(n) = \frac{1}{\overline{G}} e^{-n/\overline{G}} \frac{1}{(m-1)!} \left(\frac{n}{\overline{G}}\right)^{m-1} \quad (101)$$

The effective cluster size distribution for  $p_{clu}(n) = n_0/n^2 \Theta(n - n_0)$  is then

$$p_{clu}^G(n) = \frac{1}{\overline{G}} e^{-n/\overline{G}} \int_{n_0}^{\infty} \frac{n_0}{m^2 \Gamma(m)} \left(\frac{n}{\overline{G}}\right)^{m-1} dm \quad (102)$$

Using this effective cluster size distribution together with the distribution  $p_G(n, d)$  in Eq. B.20 we can evaluate the impact on the time resolution and have

$$\frac{\Delta_\tau^G}{\Delta_\tau} = \sqrt{\frac{w_G(d)}{w(d)}} = 1 + \varepsilon \quad (103)$$

where  $\varepsilon = 9/4.6/2.2/1.5 \times 10^{-4}$ . The effect of gain fluctuations on the time resolution is less than 0.1 % for sensors of more than  $50 \mu\text{m}$  thickness and is therefore completely negligible.

#### 5.4. Leading edge discrimination for silicon sensors with gain

In this section we discuss the time resolution when considering leading edge discrimination of sensors with gain. We proceed as in Section 4.6 and convolute the signal from a single e-h pair at position  $z$

$$i_0(x, y, z, t) = -Gqv_2 E_w(x, y, v_2(t - z/v_1)) [\Theta(t - z/v_1) - \Theta(t - z/v_1 - d/v_2)] \quad (104)$$

with the electronics delta response and find

$$\begin{aligned} g(x, y, z, t) &= \Theta(t - z/v_1) \Theta(d/v_2 + z/v_1 - t) \int_0^{\frac{v_2}{d} (1 - \frac{z}{v_1})} f\left(\frac{t - z/v_1 - ud/v_2}{t_p}\right) E\left(\frac{x}{d}, \frac{y}{d}, u, \frac{w_x}{d}, \frac{w_y}{d}, 1\right) du \\ &+ \Theta(t - d/v_2 - z/v_1) \int_0^1 f\left(\frac{t - z/v_1 - ud/v_2}{t_p}\right) E\left(\frac{x}{d}, \frac{y}{d}, u, \frac{w_x}{d}, \frac{w_y}{d}, 1\right) du \end{aligned} \quad (105)$$

which for an infinitely extended electrode with  $E_w = 1/d$  evaluates to

$$\begin{aligned} \frac{n^{n+1}}{e^n} \frac{d}{t_p} g(x, y, z, t) &= v_2 \Theta(t - z/v_1) \Theta(d/v_2 + z/v_1 - t) \left[ n! - \Gamma\left(n + 1, \frac{n(v_1 t - z)}{t_p v_1}\right) \right] \\ &- v_2 \Theta(t - d/v_2 - z/v_1) \left[ \Gamma\left(n + 1, \frac{n(v_1 t - z)}{t_p v_1}\right) - \Gamma\left(n + 1, \frac{n(t - d/v_2 - z/v_1)}{t_p}\right) \right] \end{aligned} \quad (106)$$

Evaluating Eq. 81, Eq. 82 and Eq. 83 we then find the results shown in Fig. 24a. We find that even for leading edge discrimination of the normalized signal the time resolution for a sensor with gain does not improve beyond the centroid time resolution value. The reason is that in the outlined formulas the signal is normalized by the total charge deposited in the sensor. The signal that makes up the leading edge has however no correlation with the total deposited charge but is only related to the number of electrons that

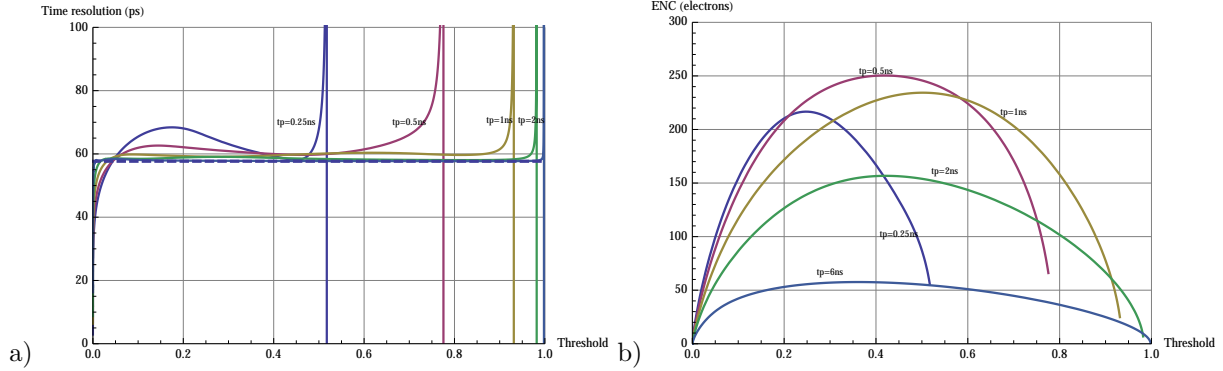


Figure 24: a) Time resolution for a gain sensor of  $50\mu\text{m}$  thickness at 200 V bias voltage when applying a threshold to the signal normalized by the total charge, assuming the Landau theory. The values do not improve beyond the centroid time resolution which is indicated by the dashed horizontal line. b) ENC needed to match the noise effect of the time resolution to the effect from the Landau fluctuations.

have already arrived at the gain layer. This is very different from the standard silicon sensor without gain, where the movement of all deposited charges makes up the leading edge signal.

If one wants to improve the time resolution of silicon sensors with gain beyond the centroid time resolution, one therefore needs ultra fast front-end electronics with slewing corrections related to the leading edge of the signal and not to the total charge of the signal. This goes beyond the mathematical formalisms developed in this report and Monte Carlo simulations have to be used to study this scenario.

## 6. Comparison with measurements

In [12] the time resolution of an LGAD sensor with  $50\mu\text{m}$  thickness is quoted as  $\sigma = 34\text{ ps}$  at 200 V and  $\sigma = 27\text{ ps}$  at 230 V. Eq. 90 predicts a centroid time resolution of  $\sigma = 32\text{ ps}$  for 200 V and  $\sigma = 31\text{ ps}$  for 230 V for the PAI model. The measured and calculated numbers are therefore in the same range, which seems to confirm the effect shown in Fig. 24, namely that even when using leading edge discrimination with electronics of  $\approx 0.5\text{ ns}$  peaking time for this sensor one is effectively measuring the centroid time.

In [6] the time resolution for multiple particles passing a 133, 211,  $285\mu\text{m}$  sensor is given. All sensors were biased at 600 V. An amplifier delta response of 1 ns peaking time is used, resulting in a peaking time for the average signal of the  $211\mu\text{m}$  sensor of  $\approx 2\text{ ns}$ . Leading edge discrimination at 50% of the signal peak is used. Eq. 20 predicts centroid time resolutions of  $\sigma = 24, 41, 60\text{ ps}$  for the three sensors when using the PAI model. With a peaking time of 1 ns and the threshold set at 50% of the signal Eq. 83 predicts a resolution of  $\sigma \approx 14\text{ ps}$ , for all three values of sensor thickness. From Eq. 27 we see that the scaling factor when having 100 MIPs instead of one MIP amounts to  $\approx 0.77$ , so we expect a time resolution of 11 ps for all these cases, which actually does approximately match the quoted number where the resolution saturates.

The NA62 Gigatracker uses a  $200\mu\text{m}$  sensor with  $300 \times 300\mu\text{m}$  pixels. The signals are read by a frontend with 5 ns peaking time and the threshold is set to around 30% of the signal. A measured time resolution of 190 ps for 200 V is quoted [1]. The effect of noise on these numbers is quoted to be negligible. To compare to calculations, we would in principle have to evaluate Eq. 82 for leading edge discrimination of a sensor with finite pixel size, which turns out to be unfeasible, so we compare to some limiting cases. The PAI model and leading edge discrimination at about 35% of the signal for 200 V predicts a time resolution

of 64 ps r.m.s. (42 ps  $\sigma$ ) for an infinitely large pad. The observed time resolution is therefore dominated by the weighting field effect. The impact of the centroid time for the weighting field (correlated with the Landau fluctuations) effect is 272 ps r.m.s. (224 ps  $\sigma$ ). The effect of leading edge discrimination on the weighting field effect, which is not discussed in this report, will reduce this number to some extent, so the measured 190 ps are in the right ballpark. For a more accurate quantitative evaluation, a Monte Carlo simulation must be performed.

In [5] a time resolution of 100 ps is reported for a sensor of 100  $\mu\text{m}$  thickness and  $800 \times 800 \mu\text{m}$  pixels, biased at 230 V. An amplifier of 200-400 ps rise-time is used and a time resolution of 100 ps is reported. The PAI model predicts a centroid time resolution of  $\sigma = 26$  ps for this sensor, and the leading edge discrimination will still result in some improvement on top of this number. As shown in the paper, the time resolution is fully dominated by the noise contribution, so we cannot extract the time resolution component due to Landau fluctuations from this measurement.

## 7. Conclusions

- The probability for a relativistic particle to deposit  $n$  e-h pairs in a silicon sensor of thickness  $d$  is given by

$$p(n, d) = \mathcal{L}^{-1} \left[ e^{d/\lambda(P_{clu}(s)-1)} \right] \quad (107)$$

where  $P_{clu}(s)$  is the Laplace transform of the cluster size distribution and  $\lambda$  is the average distance between primary collisions, which evaluates to  $\lambda \approx 0.212 \mu\text{m}$  for relativistic particles in silicon. For a  $1/n^2$  cluster size distribution this expression becomes the Landau distribution, while for a more realistic cluster size distribution from the PAI model we get a distribution with a relative width that is 25-35% smaller than the one from the Landau distribution.

- The standard deviation of the centroid time of a silicon detector signal is given by

$$\Delta_\tau = w(d/\lambda) \sqrt{\frac{4}{180} T_1^2 - \frac{7}{180} T_{12}^2 + \frac{4}{180} T_2^2} \quad (108)$$

assuming a large readout electrode and negligible depletion voltage.  $T_1 = d/v_1, T_2 = d/v_2, T_{12} = d/\sqrt{v_1 v_2}$  are the drift times of the electrons and holes. Using the Landau theory for charge deposit, the expression  $w(d/\lambda)$  approaches  $1/\sqrt{\ln d/\lambda}$  for large values of  $d$ . In the interval of  $25 < d < 500 \mu\text{m}$ ,  $w(d/\lambda)$  can be approximated by

$$w(d/\lambda) \approx \frac{1}{\sqrt{a + b \ln d/\lambda + c (\ln d/\lambda)^2}} \quad (109)$$

with  $a = 1, b = 1.155, c = 0$  for the Landau theory,  $a = 13.7, b = -4.9, c = 0.85$  for a PAI charge deposit model and  $a = 47.7, b = -22.8, c = 3.37$  when performing a Gaussian fit to the measured time distribution for the PAI model.

For a silicon sensor of 300  $\mu\text{m}$  thickness and 600 V this evaluates to a resolution of 161, 103, 64 ps, indicating that the Landau theory overestimates the fluctuations and that we have to clearly distinguish the r.m.s. and the Gaussian fit due to significant tails in the distribution. For a 200  $\mu\text{m}$  sensor at 300 V the resolution evaluates to 132, 88, 56 ps. For a 50  $\mu\text{m}$  sensor at 200 V the values are 22, 17, 12 ps.

- For multiple particles passing the silicon sensor the time resolution scales from the single particle time resolution  $\Delta_\tau(1 \text{ particle})$  as

$$\frac{\Delta_\tau(n \text{ particles})}{\Delta_\tau(1 \text{ particle})} = \frac{1}{\sqrt{1 + \frac{\ln n}{\ln d/\lambda}}} \quad (110)$$



which amounts to an improvement of only 26, 24, 23, 22% for a 50, 100, 200, 300  $\mu\text{m}$  sensor when going from 1 to 100 particles.

- Measuring the sensor signal with an amplifier of peaking time  $t_p$  larger than the drift time of electrons and holes, the amplifier output is equal to the delta response, scaled by the total signal charge and shifted by the centroid time. To determine the time of this pulse of known shape one can then use standard techniques of constant fraction discrimination and optimum filtering to extract the time information. Assuming the Landau theory, the average contribution of the noise to the time resolution is then

$$\bar{\sigma}_t = \sigma_{noise}[electrons] \frac{\lambda}{dn_0} \frac{1}{1 + 1.155 \ln d/\lambda} t_p c(n_s) \quad (111)$$

where  $t_p$  is the peaking time of the amplifier and  $c(n_s)$  is a constant depending on the measurement technique. Using constant fraction discrimination at the maximum slope of the signal we have  $c(n_s) \approx 0.55 - 0.6$ . Using continuous signal sampling and optimum filtering one arrives at similar numbers when sampling at an interval of  $t_p/2$  and one can achieve  $c(n_s) \approx 0.2 - 0.3$  for very high frequency sampling. For  $t_p = 2 \text{ ns}$ ,  $d = 50 \mu\text{m}$  and an Equivalent Noise Charge (ENC) of 50 electrons we have a contribution from the noise of  $\sigma_t \approx 17 \text{ ps}$ , that has to be added in square with the numbers from Landau fluctuations. In order to exploit the intrinsic time resolution of thin silicon sensors one therefore needs ultra low noise performance of the frontend electronics. For a given series noise voltage  $e_n$  of an amplifier, the equivalent noise charge decreases with  $1/\sqrt{t_p}$ , the effect of the noise on time resolution does however increase linearly with  $t_p$ . It is therefore advantageous to use faster electronics if power consumption allows and other noise sources do not start to become dominant.

- Assuming a square readout pixel of dimension  $w$ , the variation of the track position and therefore the variation of the weighting field and related signal shape will have an impact on the time resolution and the standard deviation of the centroid time becomes

$$\Delta_\tau = \sqrt{w(d/\lambda)^2(k_{11}T_1^2 + k_{12}T_{12}^2 + k_{22}T_2^2) + (c_{11}T_1^2 + c_{12}T_{12}^2 + c_{22}T_2^2)} \quad (112)$$

Neglecting charge fluctuations and assuming a uniform charge deposit, the coefficients  $k_{11}, k_{12}, k_{22}$  vanish. Assuming very large readout pixels, the coefficients  $c_{11}, c_{12}, c_{22}$  vanish and  $k_{11}, k_{12}, k_{22}$  become  $4/180, -7/180, 4/180$  in accordance with the above. For very small pixels, we have  $k_{11} = 1/12$  and all other coefficients vanish, which is in accordance with an arrival time distribution of charges at the pad. Landau fluctuations and weighting field fluctuations are strongly correlated, so they cannot be decoupled or 'added in squares'. Since  $k_{11} > k_{22}$ , the effect of weighting field fluctuations is smallest if  $T_1$  is small i.e. if the electrons move towards the readout pixel. In this case it seems possible that for values of  $w/d \gtrsim 1$  the weighting field effect does not add significantly to the centroid time resolution. We note that this calculation assumes perpendicular tracks and neglects diffusion.

- The expressions for leading edge discrimination of the normalized silicon sensor signal (i.e. the signal divided by the total charge) show that the centroid time resolution is indeed recovered for large peaking times, and that for faster electronics the time resolution is significantly improved when placing the threshold at  $< 40\%$  of the total signal charge. As an example, for a 50  $\mu\text{m}$  sensor at 200 V, a peaking time of 1 ns and a threshold at 30 % of the normalized signal, the time resolution improves by a factor 2 with respect to the centroid time and the noise must be less than 70 electrons in order to not significantly add to this value.

- For silicon sensors with internal gain (LGAD), the standard deviation of the centroid time becomes

$$\Delta_\tau = w(d/\lambda) \frac{T_1}{\sqrt{12}} \quad (113)$$

This formula assumes that only the gain holes contribute to the signal. This expression is the same as the one for the very small pixels without gain and represents in essence an arrival time distribution. For a  $200\mu\text{m}$  sensor at 300 V the time resolution is 255, 170, 108 ps for the Landau, PAI and Gaussfit PAI model. These numbers are a factor 2 larger compared to the sensor without gain. For a  $50\mu\text{m}$  sensor at 200 V the numbers are 57, 44, 32 ps, about a factor 2.5 larger than for the sensor without gain. The very big advantage of sensors with gain is the large signal to noise ratio that can make the noise contribution to the time resolution negligible and therefore allows large pixels, electronics with modest noise performance and modest bandwidth.

- The impact of gain fluctuations on the time resolution for sensors with internal gain (LGAD) of 50-300  $\mu\text{m}$  thickness is on the 0.1 % level and therefore negligible.
- Including the effect of the finite pixel size on the centroid time resolution of a silicon sensor with gain we find

$$\Delta_\tau = \sqrt{w(d/\lambda)^2 \frac{T_1^2}{12} + s_{22}T_2^2} \quad (114)$$

In contrast to sensors without gain there is no correlation between the Landau fluctuations and the weighting field fluctuations. For uniform charge deposit, only the second term of the expression remains. For very large and very small pads the coefficient  $s_{22}$  vanishes and the effect is largest for  $w/d \approx 3$ . In addition the expression is the same, whether the electrode at the side of the gain layer  $z = 0$  or the electrode on the opposite side is segmented into pixels.

The calculations presented in this report provide insight into some principle dependencies for the time resolution of silicon sensors on charge fluctuations, noise and weighting field fluctuations. The inclusion of more detailed models including the effect of diffusion, track angle, finite depletion voltage and pixelization are best accomplished through Monte Carlo simulations and the formulas of this report can be used as benchmarks for such studies.

## Acknowledgement

We would like to thank Heinrich Schindler for providing the data of the PAI model as well as Nicolo Cartiglia, Matthew Noy and Angelo Rivetti for important discussions.

## Appendix A.

Evaluating Eq. 3 with the specific model of the  $1/n^2$  distribution from Eq. 6 we find the Landau distribution  $L(x)$  according to

$$L(x) = \frac{1}{2\pi i} \int_{\sigma-i\infty}^{\sigma+i\infty} \exp[sx + s \ln s] ds \quad (A.1)$$

$$= \frac{1}{\pi} \int_0^\infty \exp(-\pi/2 t) \cos(tx + t \ln t) dt \quad (A.2)$$

$$= \frac{1}{\pi} \int_0^\infty \exp[-tx - t \ln t] \sin(\pi t) dt \quad (A.3)$$

Expression A.2 is well suited for evaluation for  $x < 0$ , while Eq. A.3 is well suited for evaluation for  $x > 0$ . For large values of  $x$  the Landau distribution approximates to

$$L(x) \approx \frac{1}{x^2} \quad (\text{A.4})$$

## Appendix B.

The centroid time of the silicon detector signal assuming  $n_k$  e-h pairs in slice  $k$  is

$$\tau(n_1, n_2, \dots, n_N) = \frac{1}{2d(\sum_{k=1}^N n_k)} \sum_{k=1}^N n_k \left[ \frac{z_k^2}{v_1} + \frac{(d - z_k)^2}{v_2} \right] \quad (\text{B.1})$$

The average centroid time  $\bar{\tau}$  is then given by

$$\bar{\tau} = \int_0^\infty \int_0^\infty \dots \int_0^\infty \tau(n_1, n_2, \dots, n_N) p(n_1, \Delta z) p(n_2, \Delta z) \dots p(n_N, \Delta z) dn_1 dn_2 \dots dn_N \quad (\text{B.2})$$

Since

$$\int_0^\infty \int_0^\infty \dots \int_0^\infty \frac{n_1 + n_2 + \dots + n_N}{n_1 + n_2 + \dots + n_N} p(n_1, \Delta z) p(n_2, \Delta z) \dots p(n_N, \Delta z) dn_1 dn_2 \dots dn_N = 1 \quad (\text{B.3})$$

we have

$$\int_0^\infty \int_0^\infty \dots \int_0^\infty \frac{n_k}{n_1 + n_2 + \dots + n_N} p(n_1, \Delta z) p(n_2, \Delta z) \dots p(n_N, \Delta z) dn_1 dn_2 \dots dn_N = \frac{1}{N} \quad k = 1, 2, \dots, N \quad (\text{B.4})$$

and therefore

$$\bar{\tau} = \frac{1}{2d} \sum_{k=1}^N \frac{1}{N} \left[ \frac{z_k^2}{v_1} + \frac{(d - z_k)^2}{v_2} \right] \approx \frac{1}{2d^2} \int_0^d \left[ \frac{z^2}{v_1} + \frac{(d - z)^2}{v_2} \right] dz = \frac{d}{6} \left( \frac{1}{v_1} + \frac{1}{v_2} \right) \quad (\text{B.5})$$

which is the expected centroid time of the two triangular signals from the electrons and the holes. The second moment of the centroid time  $\tau^2$  is given by

$$\overline{\tau^2} = \int_0^\infty \int_0^\infty \dots \int_0^\infty \tau^2(n_1, n_2, \dots, n_N) p(n_1, \Delta z) p(n_2, \Delta z) \dots p(n_N, \Delta z) dn_1 dn_2 \dots dn_N \quad (\text{B.6})$$

$$\tau^2(n_1, n_2, \dots, n_N) = \frac{1}{4d^2 (\sum_{k=1}^N n_k)^2} \sum_{k=1}^N \sum_{r=1}^N n_k n_r \left[ \frac{z_k^2}{v_1} + \frac{(d - z_k)^2}{v_2} \right] \left[ \frac{z_r^2}{v_1} + \frac{(d - z_r)^2}{v_2} \right] \quad (\text{B.7})$$

We define

$$\begin{aligned} a_N &= \int_0^\infty \int_0^\infty \dots \int_0^\infty \frac{n_k n_r}{(n_1 + n_2 + \dots + n_N)^2} p(n_1, \Delta z) p(n_2, \Delta z) \dots p(n_N, \Delta z) dn_1 dn_2 \dots dn_N \quad k \neq r \\ b_N &= \int_0^\infty \int_0^\infty \dots \int_0^\infty \frac{n_k^2}{(n_1 + n_2 + \dots + n_N)^2} p(n_1, \Delta z) p(n_2, \Delta z) \dots p(n_N, \Delta z) dn_1 dn_2 \dots dn_N \end{aligned} \quad (\text{B.8})$$

and since we have

$$\int_0^\infty \int_0^\infty \dots \int_0^\infty \frac{(n_1 + n_2 + \dots + n_N)^2}{(n_1 + n_2 + \dots + n_N)^2} p(n_1, \Delta z) p(n_2, \Delta z) \dots p(n_N, \Delta z) dn_1 dn_2 \dots dn_N = 1 \quad (\text{B.9})$$

it holds that

$$N b_N + N(N-1)a_N = 1 \quad \rightarrow \quad a_N = \frac{1 - N b_N}{N(N-1)} \approx \frac{1}{N^2} - \frac{b_N}{N} \quad (\text{B.10})$$

The second moment of  $\tau$  therefore becomes

$$\overline{\tau^2} = \frac{b_N}{4d^2} \sum_{k=1}^N \left[ \frac{z_k^2}{v_1} + \frac{(d-z_k)^2}{v_2} \right]^2 + \frac{a_N}{4d^2} \sum_{k=1}^N \sum_{r \neq k=1}^N \left[ \frac{z_k^2}{v_1} + \frac{(d-z_k)^2}{v_2} \right] \left[ \frac{z_r^2}{v_1} + \frac{(d-z_r)^2}{v_2} \right] \quad (\text{B.11})$$

$$= \frac{b_N - a_N}{4d^2} \sum_{k=1}^N \left[ \frac{z_k^2}{v_1} + \frac{(d-z_k)^2}{v_2} \right]^2 + \frac{a_N}{4d^2} \sum_{k=1}^N \sum_{r=1}^N \left[ \frac{z_k^2}{v_1} + \frac{(d-z_k)^2}{v_2} \right] \left[ \frac{z_r^2}{v_1} + \frac{(d-z_r)^2}{v_2} \right] \quad (\text{B.12})$$

$$\approx \frac{b_N}{4d^2} \frac{1}{\Delta z} \int_0^d \left[ \frac{z^2}{v_1} + \frac{(d-z)^2}{v_2} \right]^2 dz + \frac{a_N}{4d^2} \frac{1}{(\Delta z)^2} \left( \int_0^d \left[ \frac{z^2}{v_1} + \frac{(d-z)^2}{v_2} \right] dz \right)^2 \quad (\text{B.13})$$

$$= \frac{b_N}{\Delta z} \frac{d^3(3v_1^2 + v_1v_2 + v_2^2)}{60v_1^2v_2^2} + \frac{a_N}{(\Delta z)^2} \frac{d^4(v_1 + v_2)^2}{36v_1^2v_2^2} \quad (\text{B.14})$$

$$= \frac{b_N}{\Delta z} \frac{d^3(4v_1^2 - 7v_1v_2 + 4v_2^2)}{180v_1^2v_2^2} + \frac{d^2(v_1 + v_2)^2}{36v_1^2v_2^2} \quad (\text{B.15})$$

and we have for the variance

$$\Delta_\tau^2 = \overline{\tau^2} - \bar{\tau}^2 = \frac{b_N d}{\Delta z} \frac{d^2(4v_1^2 - 7v_1v_2 + 4v_2^2)}{180v_1^2v_2^2} \quad (\text{B.16})$$

The expression for  $\Delta_\tau$  is symmetric with respect to  $v_1$  and  $v_2$ , which reflects the fact that the induced signal on the electrode at  $z = 0$  is always equal (and opposite in sign) to the signal at the electrode at  $z = d$ . To evaluate  $b_N$

$$b_N = \int_0^\infty \int_0^\infty \dots \left[ \int_0^\infty \frac{n_1^2 p(n_1, \Delta z)}{(n_1 + n_2 + \dots + n_N)^2} dn_1 \right] p(n_2, \Delta z) \dots p(n_N, \Delta z) dn_2 \dots dn_N \quad (\text{B.17})$$

we change variables according to  $n = n_2 + n_3 + \dots + n_N$ , i.e.  $n_2 = n - n_3 - n_4 - \dots - n_N$  and  $dn_2 = dn$  and see that the expression outside the brackets becomes equal to the the  $N - 1$  times self convoluted probability  $p(n, \Delta z)$  which is simply  $p(n, d - \Delta z) \approx p(n, d)$ . Using Eq. 1 for small values of  $\Delta z$  the expression therefore becomes

$$b_N = \int_0^\infty \left[ \int_0^\infty \frac{n_1^2 p(n_1, \Delta z)}{(n_1 + n)^2} dn_1 \right] p(n, d) dn = \int_0^\infty \left[ \frac{\Delta z}{\lambda} \int_0^\infty \frac{n_1^2 p_{clu}(n_1)}{(n_1 + n)^2} dn_1 \right] p(n, d) dn \quad (\text{B.18})$$

so for the variance we finally have

$$\Delta_\tau^2 = \overline{\tau^2} - \bar{\tau}^2 = w(d)^2 \left( \frac{4d^2}{180v_2^2} - \frac{7d^2}{180v_1v_2} + \frac{4d^2}{180v_1^2} \right) \quad (\text{B.19})$$

$$w(d)^2 = \int_0^\infty \left[ \frac{d}{\lambda} \int_0^\infty \frac{n_1^2 p_{clu}(n_1)}{(n_1 + n)^2} dn_1 \right] p(n, d) dn \quad (\text{B.20})$$

This expression for  $w(d)$  is completely general for any kind of cluster size distributions  $p_{clu}(n)$  and resulting  $p(n, d)$ .

## Appendix C.

Using the Landau theory we have  $p_{clu}(n)$  from Eq. 6 and therefore

$$\int_0^\infty \frac{n_1^2 p_{clu}(n_1)}{(n_1 + n)^2} dn_1 = \int_{n_0}^\infty \frac{n_0}{(n_1 + n)^2} dn_1 = \frac{n_0}{n + n_0} \quad (C.1)$$

and with Eq. 7 we get

$$w(d)^2 = n_0 \frac{d}{\lambda} \int_0^\infty \frac{p(n, d)}{n + n_0} dn = \int_0^\infty \frac{L(z + \gamma - 1 - \ln d/\lambda)}{z + \lambda/d} dz \quad (C.2)$$

Using Eq. A.2 for  $L(x)$  we have

$$w(d)^2 = \int_0^\infty e^{-t\pi/2} \left[ \frac{1}{2} \sin(ft) - \frac{1}{\pi} \sin(ft) \text{SinIntegral}(t\lambda/d) - \frac{1}{\pi} \cos(ft) \text{CosIntegral}(t\lambda/d) \right] dt \quad (C.3)$$

with

$$f = 1 - \gamma + \lambda/d - \ln t + \ln d/\lambda \quad (C.4)$$

The integrand is 'damped' by the exponential decay where beyond  $t = 10$  the integrand will be negligible. For small values of  $\lambda/d$  we can use  $\text{SinIntegral}(x) \approx x$  and  $\text{CosIntegral}(x) \approx \gamma + \ln x$  and we get

$$w(d)^2 \approx \int_0^\infty e^{-t\pi/2} \left[ \frac{1}{2} \sin(ft) - \frac{1}{\pi} (1 - f) \cos(ft) \right] dt \quad (C.5)$$

$$f \approx 1 - \gamma - \ln t + \ln d/\lambda \quad (C.6)$$

For  $d/\lambda > 40$  the approximation is accurate to better than 1% and the dependence on  $b_N$  for different sensor values of the sensor thickness is only through  $\ln d/\lambda$ . For very large numbers of  $d/\lambda$  the expression approaches

$$w(d)^2 = \frac{1}{\ln(d/\lambda)} \quad d/\lambda \rightarrow \infty \quad (C.7)$$

For  $d/\lambda > 40$  this expression for  $w(d)$  is within 15% of the exact expression C.3.

## Appendix D.

For the convolution of the Landau distribution with a Gaussian we use Eq. A.3 and find

$$p_G(n, d) = \frac{1}{G} \int_0^\infty p(m, d) \frac{1}{\sqrt{2\pi m}} \exp\left(-\frac{(n/G - m)^2}{2m}\right) dm \quad (D.1)$$

$$\begin{aligned} &= \frac{1}{G} \int_0^\infty \left[ \frac{\lambda}{n_0 d} \frac{1}{\pi} \int_0^\infty \exp\left(-t\left(\frac{\lambda}{n_0 d} m + \gamma - 1 - \ln d/\lambda\right) - t \ln t\right) dt \right] \sin(\pi t) \frac{\exp\left(-\frac{(n/G - m)^2}{2m}\right)}{\sqrt{2\pi m}} dm \\ &= \frac{1}{G} \frac{\lambda}{n_0 d \pi} \int_0^\infty \exp\left[-t(\gamma - 1 - \ln d/\lambda) - t \ln t + n/G \left(1 - \sqrt{1 + \frac{2\lambda t}{n_0 d}}\right)\right] \frac{1}{\sqrt{1 + \frac{2\lambda t}{n_0 d}}} \sin(\pi t) dt \end{aligned} \quad (D.2)$$

## Appendix E.

The expression for the weighting potential of a rectangular pad of dimension  $w_x, w_y$  centred at  $x = y = 0$  with a parallel plate separation of  $d$  is given in [25] as

$$\phi_w(x, y, z, w_x, w_y, d) = \frac{1}{2\pi} f(x, y, z, w_x, w_y) - \frac{1}{2\pi} \sum_{n=1}^{\infty} [f(x, y, 2nd - z, w_x, w_y) - f(x, y, 2nd + z, w_x, w_y)] \quad (\text{E.1})$$

$$f(x, y, u, w_x, w_y) = \arctan\left(\frac{x_1 y_1}{u \sqrt{x_1^2 + y_1^2 + u^2}}\right) + \arctan\left(\frac{x_2 y_2}{u \sqrt{x_2^2 + y_2^2 + u^2}}\right) \quad (\text{E.2})$$

$$- \arctan\left(\frac{x_1 y_2}{u \sqrt{x_1^2 + y_2^2 + u^2}}\right) - \arctan\left(\frac{x_2 y_1}{u \sqrt{x_2^2 + y_1^2 + u^2}}\right) \quad (\text{E.3})$$

$$x_1 = x - \frac{w_x}{2} \quad x_2 = x + \frac{w_x}{2} \quad y_1 = y - \frac{w_y}{2} \quad y_2 = y + \frac{w_y}{2} \quad (\text{E.4})$$

We note that

$$\phi_w(x, y, z, w_x, w_y, d) = \phi_w\left(\frac{x}{d}, \frac{y}{d}, \frac{z}{d}, \frac{w_x}{d}, \frac{w_y}{d}, 1\right) \quad (\text{E.5})$$

The weighting field is given by

$$E_w^z(x, y, z, w_x, w_y, d) = \frac{1}{2\pi} g(x, y, z, w_x, w_y) + \frac{1}{2\pi} \sum_{n=1}^{\infty} [g(x, y, 2nd + z, w_x, w_y) + g(x, y, 2nd - z, w_x, w_y)] \quad (\text{E.6})$$

with

$$g(x, y, u, w_x, w_y) = \frac{x_1 y_1 (x_1^2 + y_1^2 + 2u^2)}{(x_1^2 + u^2)(y_1^2 + u^2) \sqrt{x_1^2 + y_1^2 + u^2}} + \frac{x_2 y_2 (x_2^2 + y_2^2 + 2u^2)}{(x_2^2 + u^2)(y_2^2 + u^2) \sqrt{x_2^2 + y_2^2 + u^2}} \\ - \frac{x_1 y_2 (x_1^2 + y_2^2 + 2u^2)}{(x_1^2 + u^2)(y_2^2 + u^2) \sqrt{x_1^2 + y_2^2 + u^2}} - \frac{x_2 y_1 (x_2^2 + y_1^2 + 2u^2)}{(x_2^2 + u^2)(y_1^2 + u^2) \sqrt{x_2^2 + y_1^2 + u^2}} \quad (\text{E.7})$$

and it holds that

$$E_w^z(x, y, z, w_x, w_y, d) = \frac{1}{d} E_w^z\left(\frac{x}{d}, \frac{y}{d}, \frac{z}{d}, \frac{w_x}{d}, \frac{w_y}{d}, 1\right) \quad (\text{E.8})$$

$w/d$	$c_{22}$	$c_{12}$	$c_{11}$	$c_{11} + c_{12} + c_{22}$
0	0	0	0	0
0.01	$6.13 \times 10^{-12}$	$-2.88 \times 10^{-9}$	$3.44 \times 10^{-7}$	$3.41 \times 10^{-7}$
0.1	$6.05 \times 10^{-8}$	$-2.75 \times 10^{-6}$	$3.18 \times 10^{-5}$	$2.91 \times 10^{-5}$
0.2	$9.28 \times 10^{-7}$	$-2.06 \times 10^{-5}$	$1.17 \times 10^{-4}$	$9.68 \times 10^{-5}$
0.25	$2.2 \times 10^{-6}$	$-3.88 \times 10^{-5}$	$1.74 \times 10^{-4}$	$1.37 \times 10^{-4}$
0.5	$2.77 \times 10^{-5}$	$-2.44 \times 10^{-4}$	$5.5 \times 10^{-4}$	$3.33 \times 10^{-4}$
1.	$2.1 \times 10^{-4}$	$-1.04 \times 10^{-3}$	$1.33 \times 10^{-3}$	$4.99 \times 10^{-4}$
1.5	$4.5 \times 10^{-4}$	$-1.78 \times 10^{-3}$	$1.81 \times 10^{-3}$	$4.86 \times 10^{-4}$
2.	$6.13 \times 10^{-4}$	$-2.18 \times 10^{-3}$	$2. \times 10^{-3}$	$4.34 \times 10^{-4}$
3.	$7.13 \times 10^{-4}$	$-2.31 \times 10^{-3}$	$1.94 \times 10^{-3}$	$3.41 \times 10^{-4}$
4.	$6.83 \times 10^{-4}$	$-2.14 \times 10^{-3}$	$1.74 \times 10^{-3}$	$2.77 \times 10^{-4}$
5.	$6.26 \times 10^{-4}$	$-1.93 \times 10^{-3}$	$1.54 \times 10^{-3}$	$2.32 \times 10^{-4}$
10	$4. \times 10^{-4}$	$-1.2 \times 10^{-3}$	$9.27 \times 10^{-4}$	$1.27 \times 10^{-4}$
20	$2.24 \times 10^{-4}$	$-6.64 \times 10^{-4}$	$5.06 \times 10^{-4}$	$6.61 \times 10^{-5}$
50	$9.56 \times 10^{-5}$	$-2.82 \times 10^{-4}$	$2.13 \times 10^{-4}$	$2.71 \times 10^{-5}$
$\infty$	0	0	0	0

Table E.1: Coefficients  $c_{11}, c_{12}, c_{22}$  from Eq. 58 for different vales of  $w/d$ , where  $w$  is the size of the square pixel and  $d$  is the thickness of the sensor.

$w/d$	$k_{22}$	$k_{12}$	$k_{11}$	$k_{11} + k_{12} + k_{22}$
0	0	0	$\frac{1}{12} = 8.33 \times 10^{-2}$	$\frac{1}{12} = 8.33 \times 10^{-2}$
0.01	$8.43 \times 10^{-8}$	$-6.43 \times 10^{-5}$	$8.33 \times 10^{-2}$	$8.32 \times 10^{-2}$
0.1	$5.37 \times 10^{-5}$	$-2.82 \times 10^{-3}$	$8.05 \times 10^{-2}$	$7.77 \times 10^{-2}$
0.2	$3.05 \times 10^{-4}$	$-7.32 \times 10^{-3}$	$7.57 \times 10^{-2}$	$6.87 \times 10^{-2}$
0.25	$5.13 \times 10^{-4}$	$-9.62 \times 10^{-3}$	$7.32 \times 10^{-2}$	$6.41 \times 10^{-2}$
0.5	$2.17 \times 10^{-3}$	$-1.94 \times 10^{-2}$	$6.18 \times 10^{-2}$	$4.46 \times 10^{-2}$
1.	$6.39 \times 10^{-3}$	$-2.96 \times 10^{-2}$	$4.73 \times 10^{-2}$	$2.41 \times 10^{-2}$
1.5	$9.82 \times 10^{-3}$	$-3.36 \times 10^{-2}$	$3.99 \times 10^{-2}$	$1.62 \times 10^{-2}$
2.	$1.22 \times 10^{-2}$	$-3.53 \times 10^{-2}$	$3.58 \times 10^{-2}$	$1.28 \times 10^{-2}$
3.	$1.51 \times 10^{-2}$	$-3.67 \times 10^{-2}$	$3.15 \times 10^{-2}$	$9.86 \times 10^{-3}$
4.	$1.68 \times 10^{-2}$	$-3.74 \times 10^{-2}$	$2.92 \times 10^{-2}$	$8.61 \times 10^{-3}$
5.	$1.78 \times 10^{-2}$	$-3.77 \times 10^{-2}$	$2.78 \times 10^{-2}$	$7.92 \times 10^{-3}$
10	$2. \times 10^{-2}$	$-3.83 \times 10^{-2}$	$2.5 \times 10^{-2}$	$6.68 \times 10^{-3}$
20	$2.12 \times 10^{-2}$	$-3.86 \times 10^{-2}$	$2.35 \times 10^{-2}$	$6.19 \times 10^{-3}$
50	$2.29 \times 10^{-2}$	$-3.84 \times 10^{-2}$	$2.2 \times 10^{-2}$	$6.44 \times 10^{-3}$
$\infty$	$\frac{4}{180} = 2.2 \times 10^{-2}$	$-\frac{7}{180} = -3.89 \times 10^{-2}$	$\frac{4}{180} = 2.2 \times 10^{-2}$	$\frac{1}{180} = 5.56 \times 10^{-3}$

Table E.2: Coefficients  $k_{11}, k_{12}, k_{22}$  from Eq. 67 for different vales of  $w/d$ , where  $w$  is the size of the square pixel and  $d$  is the thickness of the sensor.

w/d	0	0.1	0.2	0.3	0.4	0.5	1	1.5	2	2.5	3	4	5	10	20	30	40	50	$\infty$
$10^3 \times s_{22}$	0	0.03	0.12	0.27	0.54	0.76	2.6	4.0	4.8	5.2	5.2	4.9	4.2	2.7	1.6	1.3	1.1	1.0	0

Table E.3: Coefficients  $s_{22}$  from Eq. 94 for different vales of  $w/d$ , where  $w$  is the size of the square pixel and  $d$  is the thickness of the sensor.

## References

- [1] G. Aglieri Rinella et al., The NA62 Gigatracker *Nucl. Instrum. Meth. Phys. Res., Sect. A* 845 (2017), 147-149.
- [2] G. Aglieri Rinella et al., The TDCpix readout asic: A 75 ps resolution timing front-end for the Gigatracker of the NA62 experiment. Proceedings of the 2nd International Conference on Technology and Instrumentation in Particle Physics (TIPP 2011). *Physics Procedia*, 37 (2012), 1608-1617.
- [3] A. Kluge et al., The TDCpix readout asic: A 75 ps resolution timing front-end for the NA62 Gigatracker hybrid pixel detector. *Nucl. Instrum. Meth. Phys. Res., Sect. A* 732 (2013), 511-514.
- [4] M. Fiorini et al., High rate particle tracking and ultra-fast timing with a thin hybrid silicon pixel detector. *Nucl. Instrum. Meth. Phys. Res., Sect. A* 718 (2013), 270-273.
- [5] M. Benoit et al., 100ps time resolution with thin silicon pixel detectors and a SiGe HBT amplifier, 2016 JINST 11 P03011
- [6] N. Akchurin et al., On the timing performance of thin planar silicon sensors, *Nucl. Instrum. Meth. Phys. Res., Sect. A* 859 (2017), 31-36.
- [7] G. Pellegrini et al., Technology developments and first measurements of Low Gain Avalanche Detectors (LGAD) for high energy physics applications. *Nucl. Instrum. Meth. Phys. Res., Sect. A* 765 (2014), 12-16.
- [8] N. Cartiglia et al., Performance of ultra-fast silicon detectors. *J. Instr.*, 9(2), 2014.
- [9] H.F.-W. Sadrozinski et al., Ultra-fast silicon detectors. *Nucl. Instrum. Meth. Phys. Res., Sect. A* 730 (2013), 226-231.
- [10] H.F.-W. Sadrozinski et al., Sensors for ultra-fast silicon detectors. *Nucl. Instrum. Meth. Phys. Res., Sect. A* 765 (2014), 7-11.
- [11] N. Cartiglia et al., Design optimization of ultra-fast silicon detectors. *Nucl. Instrum. Meth. Phys. Res., Sect. A* 796 (2015), 141-148.
- [12] N. Cartiglia et al., Beam test results of a 16 ps timing system based on ultra-fast silicon detectors. *Nucl. Instrum. Meth. Phys. Res., Sect. A* 850 (2017), 83-88.
- [13] F. Cenna et al., Weightfield2: A fast simulator for silicon and diamond solid state detector. *Nucl. Instrum. Meth. Phys. Res., Sect. A* 796 (2015), 149-153.
- [14] N. Cartiglia et al., Tracking in 4 dimensions. *Nucl. Instrum. Meth. Phys. Res., Sect. A* 845 (2017), 47-51.
- [15] V. Sola et al., Ultra-fast silicon detectors for 4D tracking. *J. Instr.*, 12(02):C02072, 2017.
- [16] S. Parker et al., Increased speed: 3D silicon sensors; fast current amplifiers. *IEEE Trans. Nucl. Sci.*, 58(2):404-417, April 2011.
- [17] H. Spieler, Fast timing methods for semiconductor detectors. *IEEE Trans. Nucl. Sci.*, 29(3):1142-1158, June 1982.
- [18] A. Rivetti, Fast front-end electronics for semiconductor tracking detectors: Trends and perspectives. *Nucl. Instrum. Meth. Phys. Res., Sect. A* 765 (2014), 202-208.



- [19] J.H. Jungmann and R.M.A. Heeren, Emerging technologies in mass spectrometry imaging. *Journal of Proteomics*, 75(16):5077-5092, 2012.
- [20] C. Vallance et al., Fast sensors for time-of-flight imaging applications. *Physical Chemistry Chemical Physics*, 16(2):383-395, 2014.
- [21] H. Schindler, Microscopic simulation of particle detectors, CERN-THESIS-2012-208, <https://cds.cern.ch/record/1500583/>
- [22] W. W. M. Allison and J. H. Cobb, Relativistic charged particle identification by energy loss, *Ann. Rev. Nucl. Part. Sci.* 30 (1980), 253-298
- [23] Synopsis, Inc., Sentaurus Device User Guide Version D-2010.03.
- [24] W.E. Cleland, E.g. Stern, Signal processing considerations for liquid ionization calorimeters in a high rate environment, *Nucl. Instrum. Meth. Phys. Res., Sect. A* 338 (1994) 467-497
- [25] W. Riegler and G. Aglieri Rinella, Point charge potential and weighting field of a pixel or pad in a plane condenser. *Nucl. Instrum. Meth. Phys. Res., Sect. A* 767 (2014), 267-270.
- [26] C. Canali et al., *IEEE Trans. Electron Dev.* 22, 1045 (1975)